Distributed State Estimation in Power System Using Belief Propagation: Algorithms and Performance

Mirsad Cosovic, *Student Member, IEEE,* Dejan Vukobratovic, *Member, IEEE*

arXiv:1702.05781v1 [cs.IT] 19 Feb 2017

***Abstract*—We present a detailed study of the applications of factor graphs and the belief propagation (BP) algorithm to the state estimation (SE) problem. Our methodology starts with the BP solution for the linearized DC model, and use insights obtained therein to derive the BP algorithm for the non-linear AC model. Then, we make a key further step, where we present the solution in which the BP is applied sequentially over the AC model, akin to what is done by the Gauss-Newton method. The resulting BP-based Gauss-Newton algorithm has the interpretation of a fully distributed Gauss-Newton method with the same accuracy as the centralized SE, preserving a number of advantages brought in by the BP framework. The BP-based algorithms presented in this paper are fully distributed, however, they can be easily extended to the case of multi-area SE. Finally, the paper provides extensive numerical study of the proposed algorithms and gives a number of useful insights for their implementation.**

***Index Terms*—State Estimation, Electric Power System, Factor Graphs, Belief Propagation, Distributed Gauss-Newton Method**

I. Introduction

Motivation: Power systems consist of generation, transmission and consumption spread over wide geographical areas and operated from the control centers by the system operators. Maintaining normal operation conditions is of the central importance for the system operators [1, Ch. 1]. Control centers are traditionally operated in more centralized and independent fashion, which is considered inefficient according to present standards. Increase in the system size and complexity, as well as external socio-economic factors, lead to deregulation of electric power systems, implying their decentralized structure with distributed control centers. However, cooperation in control and monitoring across distributed control centers is critical for efficient system operation. Consequently, many centralized algorithms have to be redefined, requirements being distributed and computationally more efficient algorithms [2].

The system monitoring is an essential part of the control centers, providing control and optimization functionality whose efficiency relies on accurate state estimation (SE). The core of the SE is the SE algorithm that provides an estimate of the system state (i.e., the set of all complex bus voltages) based on the network topology and available measurements. Besides the SE algorithm, the SE includes several additional routines such as network topology processors, observability analysis and bad data analysis.

Traditionally, the centralized SE requires measurements across the system transmitted to a control center, where the centralized SE algorithm provides the estimate of the system. Precisely, the centralized SE algorithm typically uses the Gauss-Newton method to solve the non-linear weighted least-squares (WLS) problem [3], [4]. In contrast, decentralized SE distributes communication and computational effort across multiple control centers to estimate the global state of the system. Mainly, there are two approaches: i) distributed SE algorithms which require a global control center to exchange data with local control centers, and ii) algorithms with only local control centers [5]. Distributed SE algorithms target the same accuracy of the state estimate as it is achievable using the centralized SE algorithm.

Literature review: The mainstream approach to distributed SE algorithms exploits matrix decomposition techniques applied on the Gauss-Newton method. These algorithms usually achieve the same accuracy as the centralized SE algorithm and work with either global control center [6]–[8] or without it [9]–[12]. Recently, the SE algorithms based on distributed optimization [13], and in particular, the alternating direction method of multipliers became very popular [14]. Examples include algorithms based on convex relaxation [15], [16], and without convex relaxation [17]. In [18], the gossip-based Gauss-Newton algorithm is proposed which provides flexible communication model, but suffers from a certain performance loss compared with the centralized SE. The work in [19] presents a fully distributed SE algorithm for wide-area monitoring which provably converges to the centralized SE. We refer the reader to [20] for a detailed survey of the multi-area SE.

Proposed Approach: In this paper, we solve the SE problem using probabilistic graphical models that represent a powerful tool for modeling probabilistic systems [21]. More precisely, probabilistic graphical models provide convenient methodology to represent mutual dependencies among the system variables, such as the state variables of the power system. We represent the SE problem using a popular class of probabilistic graphical models called factor graphs and

This paper was presented in part at the IEEE International Conference on Smart Grid Communications (SmartGridComm), Sydney, Australia, November 2016; in part at the IEEE International Workshop on Signal Processing Advances in Wireless Communications (SPAWC), Edinburgh, United Kingdom, August 2016.

M. Cosovic is with Schneider Electric DMS NS, Novi Sad, Serbia (e-mail: mirsad.cosovic@schneider-electric-dms.com). D. Vukobratovic is with Department of Power, Electronic and Communications Engineering, University of Novi Sad, Novi Sad, Serbia (e-mail: dejanv@uns.ac.rs). Demo source code available online at https://github.com/mcosovic.

This paper has received funding from the EU 7th Framework Programme for research, technological development and demonstration under grant agreement no. 607774.

solve it using the belief propagation (BP) algorithm. Applying the BP algorithm on probabilistic graphical models without loops, it is possible to efficiently calculate marginal distributions or a mode of the joint distribution of the system of random variables (thus inferring their values) [21], [22]. The BP algorithm can be also applied to graphical models with loops (loopy BP) [23], although in that case, the solution is not guaranteed to converge to the correct marginals/modes of the joint distribution. BP is a fully distributed algorithm that takes probability distributions as an input, processes them, and outputs marginal probability distributions used to estimate values of state variables. This makes it a flexible solution for accommodation of distributed power sources and time-varying loads in various applications of electric power systems. Moreover, placing the SE into the probabilistic graphical modelling framework enables not only applications of efficient inference algorithms such as the BP, but also, a rich and increasing collection of useful tools for e.g., learning parameters of graphical models as well as graphical model structure itself from observed data [24].

The work in [25] provides the first demonstration of BP applied to the SE problem. Although this work is elaborate in terms of using, e.g., environmental correlation via historical data, it applies BP to a simple linearized DC model. The AC model is recently addressed in [26], where tree-reweighted BP is applied using preprocessed weights obtained by randomly sampling the space of spanning trees. The work in [27] investigates Gaussian BP convergence performance for the DC model. Although the above results provide initial insights on using BP for distributed SE, it is fair to say that a systematic analysis of applying the BP algorithm on the SE problem, and in particular for the AC model, is still missing. This paper intends to fill this gap.

Contributions: This paper provides a step-by-step guide for applications of factor graphs and the BP algorithm to the SE problem. Our methodology is to start with the simplest linearized DC model and use insights obtained therein to derive the native BP solution for the non-linear AC model. Unfortunately, closed-form expressions for certain classes of BP messages cannot be obtained, however, we present reasonable approximations that lead us to propose the AC-BP algorithm as an (approximate) BP solution for the AC model. Then, we make a key further step, where we change the perspective of our BP approach, and instead of applying the BP directly onto the non-linear AC model, we present the solution where the BP is applied sequentially over the AC model, akin to what is done by the Gauss-Newton method. The resulting Gauss-Newton BP (GN-BP) represents a BP counterpart of the Gauss-Newton method achieving the same accuracy, however, preserving a number of advantages brought in by the BP framework. For example, the proposed BP-based algorithms can be easily designed to provide asynchronous operation, could be integrated as part of real-time systems, and are flexible and easy to distribute and parallelize. That said, in this paper, we present fully-distributed BP-based algorithms (where system decomposition is done all the way to the level of the buses), while we note that the extension to the case of multi-area SE is straightforward. Finally, we close this paper by extensive numerical studies where we compare the proposed BP-based algorithms with the centralized SE, and provide a number of useful insights for their implementation.

Paper Organization: In Section II, we present basic factor graphs and BP concepts. Section III describes the centralized DC and AC SE. Section IV formulates closed form BP expressions for the DC-BP and AC-BP. In Section V, we define BP-based Gauss-Newton method, while Section VI considers the convergence performance and numerical results for the IEEE 14, IEEE 30 and IEEE 118 bus test case. Concluding remarks are included in Section VII.

II. Factor graphs and BP algorithm

Factor graphs and BP algorithm are widely used tools for probabilistic inference [21], [22]. In the standard setup, the goal of the BP algorithm is to efficiently evaluate the marginals of a system of random variables $\mathbf{x} = (x_1, \ldots, x_n)$ described via the joint probability density function $g(\mathbf{x})$. Assuming that the function $g(\mathbf{x})$ can be factorized proportionally ($\propto$) to a product of local functions:

$$g(\mathbf{x}) \propto \prod_{i=1}^{k} \psi_i(\mathcal{X}_i), \tag{1}$$

where $\mathcal{X}_i \subseteq \{x_1, \ldots, x_n\}$, the marginalization problem can be efficiently solved using BP algorithm.

The first step is forming a factor graph, which is a bipartite graph that describes the structure of the factorization (1). The factor graph structure comprises the set of factor nodes $\mathcal{F} = \{f_1, \ldots, f_k\}$, where each factor node f_i represents local function $\psi_i(\mathcal{X}_i)$ and the set of variable nodes $\mathcal{X} = \{x_1, \ldots, x_n\}$. The factor node f_i connects to the variable node x_s if and only if $x_s \in \mathcal{X}_i$ [28].

The BP algorithm on factor graphs proceeds by passing two types of messages along the edges of the factor graph: i) a variable node to a factor node, and ii) a factor node to a variable node messages. Both variable and factor nodes in a factor graph process the incoming messages and calculate outgoing messages. As a general BP rule, an output message on any edge (from any variable or factor node) depends on incoming messages from all other edges. BP messages generally represent "beliefs" about variable nodes, thus a message that arrives or departs from a certain variable node is a function (distribution) of the random variable corresponding to the variable node.

Message from a variable node to a factor node: Consider a part of a factor graph shown in Fig. 1 with a group of factor nodes $\mathcal{F}_s = \{f_i, f_w, ..., f_W\} \subseteq \mathcal{F}$ that are neighbours of the variable node $x_s \in \mathcal{X}$. The message $\mu_{x_s \to f_i}(x_s)$ from the variable node x_s to the factor node f_i is equal to the product of all incoming factor node to variable node messages arriving at all the other incident edges:

$$\mu_{x_s \to f_i}(x_s) = \prod_{f_a \in \mathcal{F}_s \setminus f_i} \mu_{f_a \to x_s}(x_s), \tag{2}$$

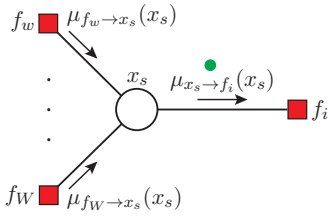

Fig. 1. Message $\mu_{x_s \to f_i}(x_s)$ from variable node x_s to factor node f_i

where $\mathcal{F}_s \setminus f_i$ represents the set of factor nodes incident to the variable node x_s, excluding the factor node f_i. Note that each message is a function of the scalar real variable x_s.

Message from a factor node to a variable node: Consider a part of a factor graph shown in Fig. 2 that consists of a group of variable nodes $\mathcal{X}_i = \{x_s, x_l, ..., x_L\} \subseteq \mathcal{X}$ that are neighbours of the factor node $f_i \in \mathcal{F}$. The

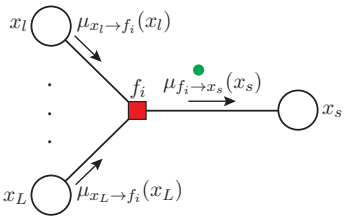

Fig. 2. Message $\mu_{f_i \to x_s}(x_s)$ from factor node f_i to variable node x_s

message $\mu_{f_i \to x_s}(x_s)$ from the factor node f_i to the variable node x_s is defined as a product of all incoming variable node to factor node messages arriving at all the other incident edges, multiplied by the function $\psi_i(\mathcal{X}_i)$ associated to the factor node f_i, and marginalized over all of the variables associated with the incoming messages:

$$\mu_{f_i \to x_s}(x_s) = \int_{x_l} \cdots \int_{x_L} \psi_i(\mathcal{X}_i) \prod_{x_b \in \mathcal{X}_i \setminus x_s} \left[\mu_{x_b \to f_i}(x_b) \cdot \mathrm{d}x_b\right], \quad (3)$$

where $\mathcal{X}_i \setminus x_s$ is the set of variable nodes incident to the factor node f_i, excluding the variable node x_s.

Marginal inference: The marginal of the variable node x_s, illustrated in Fig. 3, is obtained as the product of all incoming messages into the variable node x_s:

$$p(x_s) = \prod_{f_c \in \mathcal{F}_s} \mu_{f_c \to x_s}(x_s), \quad (4)$$

where $\mathcal{F}_s$ is the set of factor nodes incident to the variable node x_s.

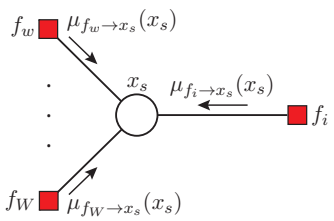

Fig. 3. Marginal inference of the variable node x_s

Here, we focus on the Gaussian BP (GBP) where all the local functions $\psi_i(\mathcal{X}_i)$ and all the inputs to the BP algorithm represent the Gaussian distribution. Due to the fact that variable node and factor node processing preserves "Gaussianity" of the messages, the resulting GBP algorithm operates exclusively with the messages representing Gaussian functions. Therefore, each message exchanged in GBP is completely represented using only two values: the mean and the variance [29].

The BP algorithm for tree-structured factor graphs (models which contain no loops) provides correct marginals. However, the BP algorithm can be also applied to factor graph with loops. In that cases, the BP may not converge, and if it does, its solution is approximate [30].

III. SE IN ELECTRIC POWER SYSTEMS

The SE in electric power systems estimates the values of the state variables based on the knowledge of network topology and parameters, and measured values obtained from measurement devices spread across the power system.

The SE assumes knowledge of the network topology and network parameters provided by the network topology processor in the form of the bus/branch model, where branches of the grid are usually described using the two-port π-model [1, Ch. 1,2]. The bus/branch model can be represented using a graph $\mathcal{G} = (\mathcal{V}, \mathcal{E})$, where the set of nodes $\mathcal{V} = \{1, \ldots, N\}$ represents the set of buses, while the set of edges $\mathcal{E} \subseteq \mathcal{V} \times \mathcal{V}$ represents the set of branches of the power network.

As an input, the SE requires a set of measurements $\mathcal{M}$ of different electrical quantities spread across various locations within the power network. Using the bus/branch model and available measurements, the observability analysis defines the measurement model [1, Ch. 4] which can be described as the system of equations [4]:

$$\mathbf{z} = \mathbf{h}(\mathbf{x}) + \mathbf{u}, \quad (5)$$

where $\mathbf{x} = (x_1, \ldots, x_n)$ is the vector of the state variables, $\mathbf{h}(\mathbf{x}) = (h_1(\mathbf{x}), \ldots, h_k(\mathbf{x}))$ is the vector of measurement functions, $\mathbf{z} = (z_1, \ldots, z_k)$ is the vector of independent measurement values, and $\mathbf{u} = (u_1, \ldots, u_k)$ is the vector of uncorrelated measurement errors. The SE problem is commonly an overdetermined system of equations $(k > n)$ [31, Sec. 2.1].

Each measurement $M_i \in \mathcal{M}$ is associated with measured value z_i, measurement error u_i and measurement function $h_i(\mathbf{x})$. Under the assumption that measurement errors u_i follow a zero-mean Gaussian distribution, the probability density function associated with the *i*-th measurement equals:

$$\mathcal{N}(z_i|\mathbf{x}, \sigma_i^2) = \frac{1}{\sqrt{2\pi\sigma_i^2}} \exp\left\{\frac{[z_i - h_i(\mathbf{x})]^2}{2\sigma_i^2}\right\}, \quad (6)$$

where σ_i^2 is the measurement variance defined by the measurement error u_i, and the measurement function $h_i(\mathbf{x})$ connects the vector of state variables $\mathbf{x}$ to the value of the *i*-th measurement.

The SE in electric power systems deals with the problem of determining state variables $\mathbf{x}$ according to the noisy observed data $\mathbf{z}$ and a prior knowledge:

$$p(\mathbf{x}|\mathbf{z}) = \frac{p(\mathbf{z}|\mathbf{x})p(\mathbf{x})}{p(\mathbf{z})}. \tag{7}$$

Assuming that the prior probability distribution $p(\mathbf{x})$ is uniform, and given that $p(\mathbf{z})$ does not depend on $\mathbf{x}$, the maximum a posteriori (MAP) solution of (7) reduces to the maximum likelihood solution, as given below [32]:

$$\hat{\mathbf{x}} = \arg\max_{\mathbf{x}} p(\mathbf{x}|\mathbf{z}) = \arg\max_{\mathbf{x}} p(\mathbf{z}|\mathbf{x}) = \arg\max_{\mathbf{x}} \mathcal{L}(\mathbf{z}|\mathbf{x}). \tag{8}$$

One can find the solution (8) via maximization of the likelihood function $\mathcal{L}(\mathbf{z}|\mathbf{x})$, which is defined via likelihoods of k independent measurements:

$$\hat{\mathbf{x}} = \arg\max_{\mathbf{x}} \mathcal{L}(\mathbf{z}|\mathbf{x}) = \arg\max_{\mathbf{x}} \prod_{i=1}^{k} \mathcal{N}(z_i|\mathbf{x}, \sigma_i^2). \tag{9}$$

It can be shown that the solution of the MAP problem can be obtained by solving the following optimization problem, known as the WLS problem [33, Sec. 9.3]:

$$\hat{\mathbf{x}} = \arg\min_{\mathbf{x}} \sum_{i=1}^{k} \frac{[z_i - h_i(\mathbf{x})]^2}{\sigma_i^2}. \tag{10}$$

The state estimate $\hat{\mathbf{x}}$ representing the solution of the optimization problem (10) is known as the WLS estimator, and is equivalent to the MAP estimator (9).

Due to the fact that each measurement $\mathcal{N}(z_i|\mathbf{x}, \sigma_i^2)$ corresponds to a limited (typically small) number of state variables $\mathbf{x}$, the above problem can be efficiently solved using probabilistic graphical modelling approach. Hence, the likelihood function $\mathcal{L}(\mathbf{z}|\mathbf{x})$ can be factorized into factors (9) affecting small subsets of state variables $\mathbf{x}$. The solution involves defining the factor graph corresponding to (9), and subsequently deriving expressions for BP messages exchanged over the factor graph, as described later in more detail.

A. AC State Estimation

The AC SE model is defined using the measurement functions $\mathbf{h}(\mathbf{x})$ that precisely follow the physical laws that connect the measured variables and the state variables. As a result, the system (5) in general represents the system of non-linear equations.

In a usual scenario, the AC SE model takes bus voltage magnitudes and bus voltage angles, transformer magnitudes of turns ratio and transformer angles of turns ratio as state variables $\mathbf{x}$. Without loss of generality, in the rest of the paper, for the AC SE we observe bus voltage angles $\boldsymbol{\theta} = (\theta_1, \dots, \theta_N)$ and bus voltage magnitudes $\mathbf{V} = (V_1, \dots, V_N)$ as state variables $\mathbf{x} \equiv (\boldsymbol{\theta}, \mathbf{V})$. Consequently, the number of state variables is $n = 2N$.

The typical set of measurements $\mathcal{M}$ in electric power systems includes: active and reactive power flow, and current magnitude, $\{M_{P_{ij}}, M_{Q_{ij}}, M_{I_{ij}}\}$, $(i,j) \in \mathcal{E}$, respectively; active and reactive power injection, $\{M_{P_i}, M_{Q_i}\}$, $i \in \mathcal{V}$; and bus voltage angle and magnitude, $\{M_{\theta_i}, M_{V_i}\}$, $i \in \mathcal{V}$. Consequently, the set of non-linear measurement functions $\mathbf{h}(\mathbf{x})$ of the AC SE model is defined as follows[1]:

The **active** and **reactive power flow** at the branch $(i,j) \in \mathcal{E}$ that connects buses i and j:

$$h_{P_{ij}}(\cdot) = V_i^2(g_{ij} + g_{si}) - V_iV_j(g_{ij}\cos\theta_{ij} + b_{ij}\sin\theta_{ij}) \tag{11a}$$
$$h_{Q_{ij}}(\cdot) = -V_i^2(b_{ij} + b_{si}) - V_iV_j(g_{ij}\sin\theta_{ij} - b_{ij}\cos\theta_{ij}), \tag{11b}$$

where V_i and V_j are bus voltage magnitudes, while $\theta_{ij} = \theta_i - \theta_j$ is the bus voltage angle difference between bus voltage angles at buses i and j. The parameters in above equations include the conductance g_{ij} and susceptance b_{ij} of the branch, as well as the conductance g_{si} and susceptance b_{si} of the branch shunt element connected at the bus i.

The **current magnitude** at the branch $(i,j) \in \mathcal{E}$ that connects buses i and j:

$$h_{I_{ij}}(\cdot) = [A_cV_i^2 + B_cV_j^2 - 2V_iV_j(C_c\cos\theta_{ij} - D_c\sin\theta_{ij})]^{1/2} \tag{12}$$
$$A_c = (g_{ij} + g_{si})^2 + (b_{ij} + b_{si})^2; \qquad B_c = g_{ij}^2 + b_{ij}^2$$
$$C_c = g_{ij}(g_{ij} + g_{si}) + b_{ij}(b_{ij} + b_{si}); \quad D_c = g_{ij}b_{si} - b_{ij}g_{si}.$$

The **active** and **reactive power injection** into the bus $i \in \mathcal{V}$:

$$h_{P_i}(\cdot) = V_i \sum_{j \in \mathcal{H}_i} V_j(G_{ij}\cos\theta_{ij} + B_{ij}\sin\theta_{ij}) \tag{13a}$$
$$h_{Q_i}(\cdot) = V_i \sum_{j \in \mathcal{H}_i} V_j(G_{ij}\sin\theta_{ij} - B_{ij}\cos\theta_{ij}), \tag{13b}$$

where $\mathcal{H}_i$ is the set of buses incident to the bus i, including the bus i. The parameters G_{ij} and B_{ij} are conductance and susceptance of the complex bus matrix [1, Sec. 2.3].

Based on the available set of measurements, the WLS estimator $\hat{\mathbf{x}} \equiv (\hat{\boldsymbol{\theta}}, \hat{\mathbf{V}})$, i.e., the solution of the WLS problem (10), can be found using the Gauss-Newton method:

$$\Big[\mathbf{J}(\mathbf{x}^\nu)^{\mathrm{T}}\mathbf{W}\mathbf{J}(\mathbf{x}^\nu)\Big]\Delta\mathbf{x}^\nu = \mathbf{J}(\mathbf{x}^\nu)^{\mathrm{T}}\mathbf{W}\mathbf{r}(\mathbf{x}^\nu) \tag{14a}$$
$$\mathbf{x}^{\nu+1} = \mathbf{x}^\nu + \Delta\mathbf{x}^\nu, \tag{14b}$$

where $\nu = \{0, 1, 2, \dots\}$ is the iteration index, $\Delta\mathbf{x}^\nu \in \mathbb{R}^n$ is the vector of increments of the state variables, $\mathbf{J}(\mathbf{x}^\nu) \in \mathbb{R}^{k \times n}$ is the Jacobian matrix of measurement functions $\mathbf{h}(\mathbf{x}^\nu)$ at $\mathbf{x} = \mathbf{x}^\nu$ (see Appendix A for details), $\mathbf{W} \in \mathbb{R}^{k \times k}$ is a diagonal matrix containing inverses of measurement variances, and $\mathbf{r}(\mathbf{x}^\nu) = \mathbf{z} - \mathbf{h}(\mathbf{x}^\nu)$ is the vector of residuals [3, Ch. 10].

B. DC State Estimation

The DC model is obtained by linearisation of the AC model. In typical operating conditions, the difference of bus voltage angles between neighbouring buses $(i,j) \in \mathcal{E}$ is very small $\theta_i - \theta_j \approx 0$, which implies $\cos\theta_{ij} \approx 1$ and $\sin\theta_{ij} \approx \theta_{ij}$. Further, all bus voltage magnitudes are $V_i \approx 1$, $i \in \mathcal{V}$, and all shunt elements and branch resistances can be neglected. This implies that the DC model ignores the reactive powers and transmission losses and takes into account only the active powers.

[1]For simplicity, we assume that the model does not contain phase-shifting transformers.

Therefore, the DC SE takes only bus voltage angles $\mathbf{x} \equiv \boldsymbol{\theta}$ as state variables. Consequently, the number of state variables is $n = N$. The DC set of measurements $\mathcal{M}$ involves only active power flow $\{M_{P_{ij}}\}$, $(i,j) \in \mathcal{E}$, active power injection $\{M_{P_i}\}$, $i \in \mathcal{V}$, and bus voltage angle $\{M_{\theta_i}\}$, $i \in \mathcal{V}$, measurements and the model is dealing with linear measurement functions $\mathbf{h}(\mathbf{x})$:

The **active power flow** at the branch $(i,j) \in \mathcal{E}$ that connects buses i and j, and the **active power injection** into the bus $i \in \mathcal{V}$ are:

$$h_{P_{ij}}(\cdot) = -b_{ij}(\theta_i - \theta_j) \tag{15a}$$

$$h_{P_i}(\cdot) = \sum_{j \in \mathcal{H}_i \setminus i} h_{P_{ij}}(\cdot), \tag{15b}$$

where $\mathcal{H}_i \setminus i$ is the set of buses incident to the bus i.

The DC state estimate $\hat{\mathbf{x}} \equiv \hat{\boldsymbol{\theta}}$, which is a solution to the WLS problem (10), is obtained through the non-iterative procedure by solving the following system of linear equations:

$$\left(\mathbf{H}^{\mathrm{T}}\mathbf{W}\mathbf{H}\right)\hat{\mathbf{x}} = \mathbf{H}^{\mathrm{T}}\mathbf{W}\mathbf{z}, \tag{16}$$

where $\mathbf{H} \in \mathbb{R}^{k \mathrm{x} N}$ is the Jacobian matrix of measurement functions (15).

IV. BP-based algorithms for the DC and AC SE

In this section, we focus on solving the DC and AC SE problems using the BP algorithm; we refer to the correspondence methods as DC-BP and AC-BP, respectively. Note that, for the DC model, the vector of state variables is $\mathbf{x} \equiv \boldsymbol{\theta}$, while the set of measurement functions is defined in Section III-B, equations (15). The AC model is characterized by the set of state variables $\mathbf{x} \equiv (\boldsymbol{\theta}, \mathbf{V})$, while measurement functions are defined in Section III-A, equations (11)-(13).

A. The factor graph construction

According to (9), in the DC scenario, the vector of state variables $\boldsymbol{\theta}$ determines the set of variable nodes $\mathcal{X} = \{\theta_1, \ldots, \theta_N\}$, while in the AC scenario, the set of state variables $\boldsymbol{\theta}$ and $\mathbf{V}$ determines the set of variable nodes $\mathcal{X} = \{(\theta_1, V_1), \ \ldots, \ (\theta_N, V_N)\}$. The set of measurements $\mathcal{M}$ defines the set of factor nodes $\mathcal{F} = \{f_1, \ldots, f_k\}$. More precisely, measurements define likelihood functions $\mathcal{N}(z_i|\mathbf{x}, \sigma_i^2)$ that in turn equal to local functions $\psi_i(\mathcal{X}_i)$ associated to factor nodes. A factor node f_i connects to a variable node $x_s \in \mathcal{X}$ if and only if the state variable x_s is an argument of the corresponding measurement function $h_i(\mathbf{x})$.

Example 4.1 (Constructing factor graph): In this example, using a simple 3-bus model presented in Fig. 4a, we demonstrate the conversion from a bus/branch model with a given measurement configuration into the corresponding factor graph for the DC and AC model. The variable nodes represent state variables, i.e., $\mathcal{X} = \{\theta_1, \ \theta_2, \ \theta_3\}$ or $\mathcal{X} = \{\theta_1, V_1, \ \ \theta_2, V_2, \ \ \theta_3, V_3\}$. Factor nodes are defined by corresponding measurements, where in our example, measurements $M_{P_{12}}$ and M_{P_3} are mapped into factor nodes $\mathcal{F} = \{f_{P_{12}}, f_{P_3}\}$. △

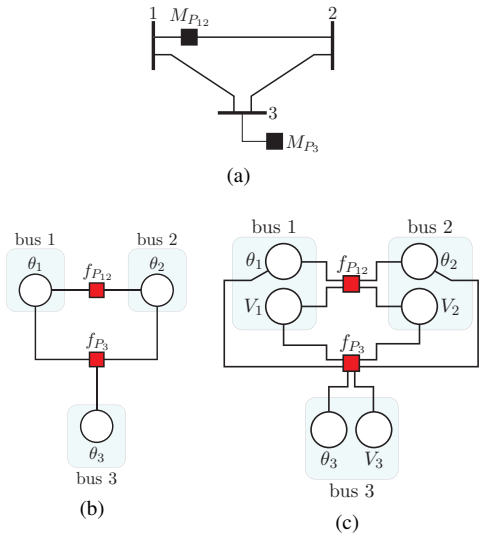

Fig. 4. Transformation of the bus/branch model and measurement configuration (subfigure a) into the corresponding factor graph for the DC model (subfigure b) and the AC model (subfigure c)

B. Derivation of BP messages

Message from a variable node to a factor node: Let us assume, for the time being, that the incoming messages $\mu_{f_w \to x_s}(x_s), \ \ldots, \ \mu_{f_W \to x_s}(x_s)$ into the variable node x_s are Gaussian and represented by their mean-variance pairs $(z_{f_w \to x_s}, \sigma^2_{f_w \to x_s}), \ \ldots, \ (z_{f_W \to x_s}, \sigma^2_{f_W \to x_s})$. Note that these messages carry beliefs about the variable node x_s provided by its neighbouring factor nodes $\mathcal{F}_s \setminus f_i$.

According to (2), it can be shown that the message $\mu_{x_s \to f_i}(x_s)$ from the variable node x_s to the factor node f_i is proportional (i.e. $\propto$) by the Gaussian function:

$$\mu_{x_s \to f_i}(x_s) \propto \mathcal{N}(z_{x_s \to f_i}|x_s, \sigma^2_{x_s \to f_i}), \tag{17}$$

with mean $z_{x_s \to f_i}$ and variance $\sigma^2_{x_s \to f_i}$ obtained as:

$$z_{x_s \to f_i} = \left(\sum_{f_a \in \mathcal{F}_s \setminus f_i} \frac{z_{f_a \to x_s}}{\sigma^2_{f_a \to x_s}} \right) \sigma^2_{x_s \to f_i} \tag{18a}$$

$$\frac{1}{\sigma^2_{x_s \to f_i}} = \sum_{f_a \in \mathcal{F}_s \setminus f_i} \frac{1}{\sigma^2_{f_a \to x_s}}. \tag{18b}$$

After the variable node x_s receives the messages from all of the neighbouring factor nodes from the set $\mathcal{F}_s \setminus f_i$, it evaluates the message $\mu_{x_s \to f_i}(x_s)$ according to (18) and sends it to the factor node f_i. Note that, due to the fact that variable node output messages do not depend on measurement functions (see equation (2)), relations (17) and (18) hold for both DC-BP and AC-BP.

Message from a factor node to a variable node: Due to dependence on the form of measurement functions $h_i(\cdot)$, the messages $\mu_{f_i \to x_s}(x_s)$ for DC-BP and AC-BP will be different. For the DC-BP, due to linearity of measurement functions $h_i(\cdot)$, closed form expressions for these messages are easy to obtain and follow a Gaussian form:

$$\mu_{f_i \to x_s}(x_s) \propto \mathcal{N}(z_{f_i \to x_s}|x_s, \sigma^2_{f_i \to x_s}). \tag{19}$$

Further, due to non-linear measurement functions $h_i(\cdot)$, the integral in (3) for the AC-BP cannot be evaluated in closed form. Consequently, the message from a factor node to a variable node will not be Gaussian.

In the following, *as an approximation*, we assume that for the AC-BP, the message $\mu_{f_i\to x_s}(x_s)$ also has the Gaussian form (19). Under this assumption, we derive the mean value and the variance of message $\mu_{f_i\to x_s}(x_s)$ for both DC-BP and AC-BP. We first present derivations for mean values and then provide expressions for variances. In both cases, we first provide exact expressions for the DC-BP, and then provide arguments that lead us to approximations used to derive messages for the AC-BP.

The message $\mu_{f_i\to x_s}(x_s)$ can be computed only when all other incoming messages (variable to factor node messages) are known. Let us assume that the messages into factor nodes are Gaussian, denoted by:

$$\begin{aligned}\mu_{x_l\to f_i}(x_l) &\propto \mathcal{N}(z_{x_l\to f_i}|x_l,\sigma^2_{x_l\to f_i})\\ &\vdots\\ \mu_{x_L\to f_i}(x_L) &\propto \mathcal{N}(z_{x_L\to f_i}|x_L,\sigma^2_{x_L\to f_i}).\end{aligned} \tag{20}$$

The Gaussian function associated with the factor node f_i is given by (Section III, equation (6)):

$$\begin{aligned}&\mathcal{N}(z_i|x_s,x_l,\ldots,x_L,\sigma_i^2)\\ &\qquad\propto \exp\left\{\frac{[z_i-h_i(x_s,x_l,\ldots,x_L)]^2}{2\sigma_i^2}\right\}.\end{aligned} \tag{21}$$

Mean value evaluation: With the DC model, only linear measurement functions are present. Hence, a measurement function can be represented in a general form as:

$$h_i(x_s,x_l,\ldots,x_L)=C_{x_s}x_s+\sum_{x_b\in\mathcal{X}_i\setminus x_s}C_{x_b}x_b, \tag{22}$$

where $\mathcal{X}_i\setminus x_s$ is the set of variable nodes incident to the factor node f_i, excluding the variable node x_s. From the expression (3), and using (20)-(22), it can be shown that the message $\mu_{f_i\to x_s}(x_s)$ from the factor node f_i to the variable node x_s is represented by the Gaussian function (19). Thus for the DC-BP, the expression for the mean $z_{f_i\to x_s}$ is *exact* and equals:

$$z_{f_i\to x_s}=\frac{1}{C_{x_s}}\left(z_i-\sum_{x_b\in\mathcal{X}_i\setminus x_s}C_{x_b}z_{x_b\to f_i}\right). \tag{23}$$

Although the expression above is obtained by directly evaluating (3) for the linear DC model, we note that it has a useful interpretation via conditional expectation. For that purpose, let us define a vector $\mathbf{x}_b=\mathcal{X}_i\setminus x_s$, and let $\mathbf{z}_{\mathbf{x}_b\to f_i}$ denote a vector of mean values of messages from variable nodes $\mathcal{X}_i\setminus x_s$ to the factor node f_i. Then, the conditional expectation $\mathbb{E}[h_i(x_s,\mathbf{x}_b)|\mathbf{x}_b=\mathbf{z}_{\mathbf{x}_b\to f_i}]$ can be calculated as:

$$\begin{aligned}&\mathbb{E}[h_i(x_s,\mathbf{x}_b)|\mathbf{x}_b=\mathbf{z}_{\mathbf{x}_b\to f_i}]\\ &=C_{x_s}\mathbb{E}[x_s|\mathbf{x}_b=\mathbf{z}_{\mathbf{x}_b\to f_i}]+\sum_{x_b\in\mathcal{X}_i\setminus x_s}C_{x_b}z_{x_b\to f_i}=z_i.\end{aligned} \tag{24}$$

From the BP perspective, the conditional expected value $\mathbb{E}[x_s|\mathbf{x}_b=\mathbf{z}_{\mathbf{x}_b\to f_i}]$ represents the mean $z_{f_i\to x_s}$. Hence, it is possible to define the conditional expectation of non-linear measurement function $h_i(\cdot)$:

$$\mathbb{E}[h_i(x_s,\mathbf{x}_b)|\mathbf{x}_b=\mathbf{z}_{\mathbf{x}_b\to f_i}]=z_i. \tag{25}$$

Due different forms of non-linear measurement functions $h_i(\cdot)$, see equations (11)-(13), the equation (25) will produce different forms of conditional expectation $\mathbb{E}[x_s|\mathbf{z}_{\mathbf{x}_b\to f_i}]\equiv z_{f_i\to x_s}$:

$$a\mathbb{E}[x_s|\mathbf{z}_{\mathbf{x}_b\to f_i}]+b=0 \tag{26a}$$

$$a\mathbb{E}[x_s^2|\mathbf{x}_b=\mathbf{z}_{\mathbf{x}_b\to f_i}]+b\mathbb{E}[x_s|\mathbf{x}_b=\mathbf{z}_{\mathbf{x}_b\to f_i}]+c=0 \tag{26b}$$

$$a\mathbb{E}[\sin^2 x_s|\mathbf{x}_b=\mathbf{z}_{\mathbf{x}_b\to f_i}]+b\mathbb{E}[\sin x_s|\mathbf{x}_b=\mathbf{z}_{\mathbf{x}_b\to f_i}]+c=0, \tag{26c}$$

where a, b and c are coefficients derived from non-linear measurement functions (see Appendix B for details).

Due to quadratic form of (26b) and (26c), we may obtain two possible values for the mean value $z_{f_i\to x_s}$. Thus in order to unambiguously define $z_{f_i\to x_s}$, we assume that certain a priori knowledge of state variables, denoted as $\widetilde{\mathbf{x}}\equiv(\widetilde{\boldsymbol{\theta}},\widetilde{\mathbf{V}})$, is available (e.g., historical data). Given the prior data, we evaluate the mean value as:

$$z_{f_i\to x_s}=\begin{cases}z^{(1)}_{f_i\to x_s}, & \text{if } \Delta>0 \text{ and } d_1<d_2\\ z^{(2)}_{f_i\to x_s}, & \text{if } \Delta>0 \text{ and } d_1>d_2\\ \widetilde{x}_s, & \text{if } \Delta<0\end{cases} \tag{27}$$

where Δ is the discriminant of the quadratic polynomial, and $d_1=|z^{(1)}_{f_i\to x_s}-\widetilde{x}_s|$, $d_2=|z^{(2)}_{f_i\to x_s}-\widetilde{x}_s|$, (see Appendix B for details).

The variance evaluation: For the DC-BP, it can be shown that the variance $\sigma^2_{f_i\to x_s}$ of Gaussian form (19) is given as:

$$\sigma^2_{f_i\to x_s}=\frac{1}{C^2_{x_s}}\left(\sigma_i^2+\sum_{x_b\in\mathcal{X}_i\setminus x_s}C^2_{x_b}\sigma^2_{x_b\to f_i}\right). \tag{28}$$

Let us provide another interpretation of the variance $\sigma^2_{f_i\to x_s}$. For this purpose, we observe the factor graph presented in Fig. 5. Consider the set of messages

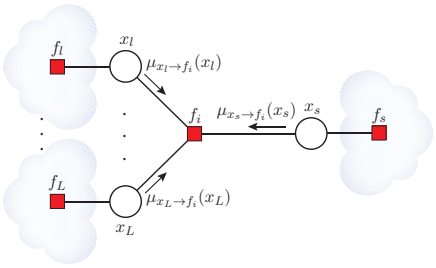

Fig. 5. Factor graph which provides interpretation of the variance $\sigma^2_{f_i\to x_s}$.

$\mu_{x_b\to f_i}=\mathcal{N}(z_{x_b\to f_i}|x_b,\sigma^2_{x_b\to f_i})$ arriving to the factor node f_i from any variable node neighbour $x_b\in\mathcal{X}_i$. Informally, we note that this message carries a "belief" about itself that the variable node x_b sends to the factor node f_i, representing collective evidence the rest of the factor graph provides about the variable node x_b. Let us represent this belief by an equivalent factor node attached to each variable node. Thus

for a set of variable nodes $\mathcal{X}_i$, we introduce a set of factor nodes $\mathcal{F}_{eq} = \{f_s,\, f_l,\, \ldots,\, f_L\}$, where for each $x_b \in \mathcal{X}_i$, the corresponding factor node $f_b \in \mathcal{F}_{eq}$ is singly-connected to x_b and by $\mathcal{N}(z_{x_b \to f_i} | x_b, \sigma^2_{x_b \to f_i})$. Note that, from the perspective of SE, this factor node can observed as a measurement defined by the value $z_{x_b \to f_i}$, variance $\sigma^2_{x_b \to f_i}$, and measurement function $h_b(x_b) = x_b$.

Let us now solve the system illustrated in Fig. 5 using the WLS method. It is easy to show that the corresponding Jacobian matrix[2] $\mathbf{H}$ and weighted matrix $\mathbf{W}$ have the following form:

$$\mathbf{H} = \begin{pmatrix} C_{x_s} & C_{x_l} & \ldots & C_{x_L} \\ 1 & 0 & \ldots & 0 \\ 0 & 1 & \ldots & 0 \\ \vdots & \vdots & & \vdots \\ 0 & 0 & \ldots & 1 \end{pmatrix} \tag{29}$$

$$\mathbf{W} = \mathrm{diag}(1/\sigma_i^2, 1/\sigma^2_{x_s \to f_i}, 1/\sigma^2_{x_l \to f_i}, \ldots, 1/\sigma^2_{x_L \to f_i}). \tag{30}$$

A variance-covariance matrix of WLS method is defined as:

$$\begin{aligned} \mathbb{V}(\mathbf{x}_i) &= (\mathbf{H}^{\mathrm{T}}\mathbf{W}\mathbf{H})^{-1} \\ &= \begin{pmatrix} \mathrm{var}(x_s) & \mathrm{cov}(x_s, x_l) & \ldots & \mathrm{cov}(x_s, x_L) \\ \mathrm{cov}(x_l, x_s) & \mathrm{var}(x_l) & \ldots & \mathrm{cov}(x_l, x_L) \\ \vdots & \vdots & & \vdots \\ \mathrm{cov}(x_L, x_s) & \mathrm{cov}(x_L, x_l) & \ldots & \mathrm{var}(x_L) \end{pmatrix}. \end{aligned} \tag{31}$$

According to (31), and using (29) and (30), the variance $\mathrm{var}(x_s)$ is:

$$\frac{1}{\mathrm{var}(x_s)} = \frac{1}{\sigma^2_{x_s \to f_i}} + \left[\frac{1}{C^2_{x_s}} \Big(\sigma_i^2 + \sum_{x_b \in \mathcal{X}_i \setminus x_s} C^2_{x_b} \sigma^2_{x_b \to f_i} \Big) \right]^{-1}. \tag{32}$$

Consider the second term on the right-hand side of (32). Recall that it represents the inverse of the variance $\sigma^2_{f_i \to x_s}$ of the message from the factor node f_i to the variable node x_s, as defined by (28). Therefore, we have demonstrated that by applying WLS on the factor graph in Fig. 5, one can obtain the expression for the variance of the message from the factor node f_i to the variable node x_s.

For the AC SE that deals with non-linear measurement functions, it is possible to define a linear approximation of the variance-covariance matrix at a given point $\mathbf{x}_i$ using the Gauss-Newton method (14a):

$$\mathbb{V}(\mathbf{x}_i) = [\mathbf{J}(\mathbf{x}_i)^{\mathrm{T}} \mathbf{W} \mathbf{J}(\mathbf{x}_i)]^{-1}. \tag{33}$$

It can be shown, using (33), that the variance $\sigma^2_{f_i \to x_s}$ is governed by (28) where the coefficients C_{x_p}, $x_p \in \mathcal{X}_i$ are defined by Jacobian elements (see Appendix A and B for details):

$$C_{x_p} = \left. \frac{\partial h_i(\cdot)}{\partial x_p} \right|_{\substack{x_s = z_{f_i \to x_s} \\ \mathbf{x}_b = \mathbf{z}_{\mathbf{x}_b \to f_i}}}. \tag{34}$$

Note that the coefficients above are evaluated at the point $\mathbf{x}_i = (x_s, \mathbf{x}_b)$, where the values in $\mathbf{x}_i$ represent the mean-values of the corresponding messages.

[2]Note that the measurement function of the factor node f_i is given by (22), while for all other factor nodes $f_b \in \mathcal{F}_{eq}$, it is equal to $h_b(x_b) = x_b$.

To summarize, for the DC-BP, after the factor node f_i receives the messages from all of the neighbouring variable nodes from the set $\mathcal{X}_i \setminus x_s$, it evaluates the message $\mu_{f_i \to x_s}(x_s)$ according to (23) and (28), and sends it to the variable node x_s. The message evaluation for the AC-BP is governed by (26) and (28), where coefficients are obtained using (34).

Marginal inference: It can be shown that the marginal of the state variable x_s, according to (4), is represented by the Gaussian function:

$$p(x_s) \propto \mathcal{N}(\hat{x}_s | x_s, \sigma^2_{x_s}), \tag{35}$$

with the mean value $\hat{x}_s$ and variance $\sigma^2_{x_s}$:

$$\hat{x}_s = \left(\sum_{f_c \in \mathcal{F}_s} \frac{z_{f_c \to x_s}}{\sigma^2_{f_c \to x_s}} \right) \sigma^2_{x_s} \tag{36a}$$

$$\frac{1}{\sigma^2_{x_s}} = \sum_{f_c \in \mathcal{F}_s} \frac{1}{\sigma^2_{f_c \to x_s}}. \tag{36b}$$

Finally, the mean-value $\hat{x}_s$ is adopted as the estimated value of the state variable x_s. In addition, note that the variance $\sigma^2_{x_s}$ of the marginal preserves the form of the WLS solution for the variance $\mathrm{var}(x_s)$ of the state variable x_s, given by (32).

C. Iterative DC-BP and AC-BP algorithms

The SE scenario is in general an instance of Loopy BP since the corresponding factor graph usually contains cycles. Loopy BP is an iterative algorithm, with an iteration index $\rho = \{0, 1, 2, \ldots\}$, and requires a message-passing schedule. The scheduling where messages from variable to factor nodes, and messages from factor nodes to variable nodes, are updated in parallel in respective half-iterations, is known as synchronous scheduling. Synchronous scheduling updates all messages in a given iteration using the output of the previous iteration as an input [34].

To present the algorithm precisely, we need to introduce different types of factor nodes. The *indirect factor nodes* $\mathcal{F}_{ind} \subset \mathcal{F}$ correspond to measurements that measure state variables indirectly. In our scenario, examples include measurements of power flows, power injections and currents. The *direct factor nodes* $\mathcal{F}_{dir} \subset \mathcal{F}$ correspond to the measurements that measure state variables directly. For our choice of state variables, an examples include measurements of voltage magnitudes and angles.

Besides direct and indirect factor nodes, we define three additional types of singly-connected factor nodes. The *slack factor node* corresponds to the slack or reference bus where the voltage angle has a given value. The *initialization factor node* is required to initialize the algorithm at certain variable nodes. Finally, the *virtual factor node* is used if the variable node is not directly measured and is singly-connected to the rest of the factor graph. Both initialization and virtual factor nodes take the value of "flat start" with variance $\sigma^2_{x_i} \to \infty$, $i \in \mathcal{V}$ or a priori given value of mean and variance of state variables.

We refer to direct factor nodes and three additional types of singly-connected factor nodes as local factor nodes

$\mathcal{F}_{loc} \subset \mathcal{F}$. Each variable node in the initialization step of the algorithm has the corresponding local factor node attached. Local factor nodes only send, but do not receive, the message to incident variable nodes. Direct and virtual factor nodes repeatedly transmit the same message to the corresponding variable node throughout BP iterations.

Algorithm 1 The DC-BP and AC-BP

procedure INITIALIZATION $\rho = 0$
  for Each $f_s \in \mathcal{F}_{loc}$ **do**
    send $\mu^{\{0\}}_{f_s \to x_s}$ to incidence $x_s \in \mathcal{X}$
  end for
  for Each $x_s \in \mathcal{X}$ **do**
    send $\mu^{\{0\}}_{x_s \to f_i} = \mu^{\{0\}}_{f_s \to x_s}$, to incidence $f_i \in \mathcal{F}_{id}$
  end for
  if AC-BP **then**
    for Each $f_i \in \mathcal{F}_{ind}$ **do**
      send $\mu^{\{0\}}_{f_i \to x_s} = \mu^{\{0\}}_{x_s \to f_i}$ to incidence $x_s \in \mathcal{X}$
    end for
  end if
end procedure
procedure ITERATION LOOP $\rho = 1, 2, \ldots$
  while stopping criterion is not met **do**
    for Each $f_i \in \mathcal{F}_{ind}$ **do**
      if DC-BP **then**
        Compute $\mu^{\{\rho\}}_{f_i \to x_s}$ using (23)*, (28)*
      end if
      if AC-BP **then**
        Compute $\mu^{\{\rho\}}_{f_i \to x_s}$ using (26)*, (28)*
      end if
    end for
    for Each $x_s \in \mathcal{X}$ **do**
      Compute $\mu^{\{\rho\}}_{x_s \to f_i}$ using (18)
    end for
  end while
end procedure
procedure OUTPUT
  for Each $x_s \in \mathcal{X}$ **do**
    Compute $\hat{x}_s$, $\sigma^2_{x_s}$ using (36)
  end for
end procedure
*Incomming messages are obtained in previous iteration $\rho - 1$

Example 4.2 (Different types of factor nodes): In this example, we consider the bus/branch model with five measurements illustrated in Fig. 6a that we use to describe different types of factor nodes. The corresponding factor graph is given in Fig. 6b, with indirect factor nodes (red squares), direct factor nodes (orange squares), the initialization factor node (green square) and the virtual factor node (blue square). △

The DC-BP and AC-BP algorithms are presented in Algorithm 1. Note that, the initialization step for the DC-BP and AC-BP is different. This is due to the fact that the variance of the message from a factor node to a variable node for the AC-BP depends not only on the mean values of incoming messages, but also on the mean value of the message whose variance is being calculated.

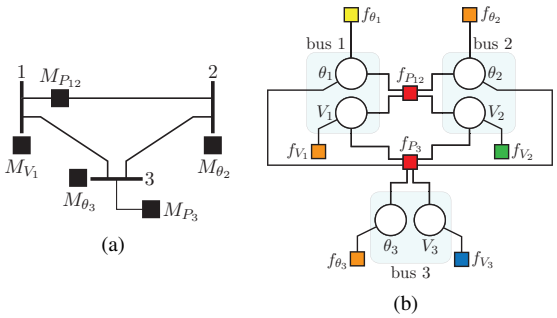

Fig. 6. Transformation of the bus/branch model and measurement configuration (subfigure a) into the corresponding factor graph with different types of factor nodes for the AC model (subfigure b)

V. DISTRIBUTED GAUSS-NEWTON BP METHOD

Unlike the previous section, where we applied the BP directly onto the non-linear AC model, in this section, we present the Gauss-Newton BP (GN-BP) method in which the BP is applied sequentially over the AC model.

Consider the Gauss-Newton method (14) where, at each iteration step ν, the algorithm returns a new estimate of $\mathbf{x}$ denoted as $\mathbf{x}^\nu$. Note that, after a given iteration, an estimate $\mathbf{x}^\nu$ is a vector of known (constant) values. If the Jacobian matrix $\mathbf{J}(\mathbf{x}^\nu)$ has a full column rank, the equation (14a) represents the linear WLS solution of the minimization problem [35]:

$$\min_{\Delta\mathbf{x}^\nu} ||\mathbf{W}^{1/2}[\mathbf{r}(\mathbf{x}^\nu) - \mathbf{J}(\mathbf{x}^\nu)\Delta\mathbf{x}^\nu]||_2^2. \tag{37}$$

Hence, at each iteration step ν, the Gauss-Newton method produces WLS solution of the following system of linear equations:

$$\mathbf{r}(\mathbf{x}^\nu) = \mathbf{g}(\Delta\mathbf{x}^\nu) + \mathbf{u}, \tag{38}$$

where $\mathbf{g}(\Delta\mathbf{x}^\nu) = \mathbf{J}(\mathbf{x}^\nu)\Delta\mathbf{x}^\nu$ comprises linear functions. The equation (14a) is the weighted normal equation for the minimization problem defined as (37), or alternatively, equation (14a) is a WLS solution of (38).

Consequently, the probability density function associated with the *i*-th measurement (i.e., the *i*-th residual component r_i) at any iteration step ν:

$$\mathcal{N}(r_i(\mathbf{x}^\nu)|\Delta\mathbf{x}^\nu, \sigma_i^2) = \frac{1}{\sqrt{2\pi\sigma_i^2}} \exp\left\{\frac{[r_i(\mathbf{x}^\nu) - g_i(\Delta\mathbf{x}^\nu)]^2}{2\sigma_i^2}\right\}. \tag{39}$$

The MAP solution of (9) can be redefined as an iterative optimization problem where, instead of solving (14), we solve MAP (sub)problem:

$$\begin{aligned}\Delta\hat{\mathbf{x}}^\nu &= \arg\max_{\Delta\mathbf{x}^\nu} \mathcal{L}\Big(\mathbf{r}(\mathbf{x}^\nu)|\Delta\mathbf{x}^\nu\Big) \\ &= \arg\max_{\Delta\mathbf{x}^\nu} \prod_{i=1}^{k} \mathcal{N}\Big(r_i(\mathbf{x}^\nu)|\Delta\mathbf{x}^\nu, \sigma_i^2\Big) \qquad (40a)\\ \mathbf{x}^{\nu+1} &= \mathbf{x}^\nu + \Delta\hat{\mathbf{x}}^\nu. \qquad (40b)\end{aligned}$$

As we show next, the solution to the above MAP sub-problem (40a) over increment variables $\Delta\mathbf{x}^{\nu}$ can be efficiently obtained using the BP algorithm applied over the underlying factor graph.

Note that, if the factor graph corresponding to the problem (40) is a tree, the resulting BP algorithm provides a solution equal to the linear WLS solution $\Delta\mathbf{x}^{\nu}$ of (14a). In general, if the factor graph contains loops, the BP solution of $\Delta\hat{\mathbf{x}}^{\nu}$ in each iteration ν (outer iteration loop) will be obtained via iterative BP algorithm (inner iteration loops). Every inner BP iteration $\rho = 1, 2, \ldots, \tau(\nu)$ outputs $\Delta\hat{\mathbf{x}}^{\nu,\rho}$, where $\tau(\nu)$ is the number of inner BP iterations within outer iteration ν.

A. The factor graph construction

From the factorization of the likelihood expression (40a), one easily obtain the factor graph corresponding to the GN-BP method as follows. The increments $\Delta\mathbf{x}$ of state variables $\mathbf{x}$ determine the set of variable nodes $\mathcal{X} = \{(\Delta\theta_1, \Delta V_1), \ldots, (\Delta\theta_N, \Delta V_N)\}$ and each likelihood function $\mathcal{N}(r_i(\mathbf{x}^{\nu})|\Delta\mathbf{x}^{\nu}, \sigma_i^2)$ represents the local function $\psi(\mathcal{X}_i)$. Since the residual equals $r_i(\mathbf{x}^{\nu}) = z_i - h_i(\mathbf{x}^{\nu})$, in general, the set of factor nodes $\mathcal{F} = \{f_1, \ldots, f_k\}$ is defined by the set of measurements $\mathcal{M}$. The factor node f_i connects to the variable node $\Delta x_s \in \{\Delta\theta_s, \Delta V_s\}$ iff the increment of the state variable Δx_s is an argument of the corresponding function $g_i(\Delta\mathbf{x})$, which is equivalent to say that the corresponding state variable $x_s \in \{\theta_s, V_s\}$ is an argument of the measurement function $h_i(\mathbf{x})$.

B. Derivation of BP messages

Message from a variable node to a factor node: It can be shown that the message $\mu_{\Delta x_s \to f_i}(\Delta x_s)$ is represented by the Gaussian function:

$$\mu_{\Delta x_s \to f_i}(\Delta x_s) \propto \mathcal{N}(r_{\Delta x_s \to f_i}|\Delta x_s, \sigma^2_{\Delta x_s \to f_i}), \tag{41}$$

with mean $r_{\Delta x_s \to f_i}$ and variance $\sigma^2_{\Delta x_s \to f_i}$:

$$r_{\Delta x_s \to f_i} = \left(\sum_{f_a \in \mathcal{F}_s \setminus f_i} \frac{r_{f_a \to \Delta x_s}}{\sigma^2_{f_a \to \Delta x_s}} \right) \sigma^2_{\Delta x_s \to f_i} \tag{42a}$$

$$\frac{1}{\sigma^2_{\Delta x_s \to f_i}} = \sum_{f_a \in \mathcal{F}_s \setminus f_i} \frac{1}{\sigma^2_{f_a \to \Delta x_s}}. \tag{42b}$$

Message from a factor node to a variable node: It can be shown that the message $\mu_{f_i \to \Delta x_s}(\Delta x_s)$ is represented by the Gaussian function:

$$\mu_{f_i \to \Delta x_s}(\Delta x_s) \propto \mathcal{N}(r_{f_i \to \Delta x_s}|\Delta x_s, \sigma^2_{f_i \to \Delta x_s}), \tag{43}$$

with mean $r_{f_i \to \Delta x_s}$ and variance $\sigma^2_{f_i \to \Delta x_s}$:

$$r_{f_i \to \Delta x_s} = \frac{1}{C_{\Delta x_s}} \left(r_i - \sum_{\Delta x_b \in \mathcal{X}_i \setminus \Delta x_s} C_{\Delta x_b} \cdot r_{\Delta x_b \to f_i} \right) \tag{44a}$$

$$\sigma^2_{f_i \to \Delta x_s} = \frac{1}{C^2_{\Delta x_s}} \left(\sigma_i^2 + \sum_{\Delta x_b \in \mathcal{X}_i \setminus \Delta x_s} C^2_{\Delta x_b} \cdot \sigma^2_{\Delta x_b \to f_i} \right). \tag{44b}$$

Algorithm 2 The GN-BP

procedure INITIALIZATION $\nu = 0$
  for Each $x_s \in \mathcal{X}$ **do**
    Initialize value of $x_s^{\{0\}}$, typically as a "flat start"
  end for
end procedure
procedure OUTER ITERATION LOOP $\nu = 0, 1, 2, \ldots; \rho = 0$
  while stopping criterion for the outer loop is not met **do**
    for Each $f_s \in \mathcal{F}_{dir}$ **do**
      compute residual $r_s^{\{\nu\}} = z_s - x_s^{\{\nu\}}$
    end for
    for Each $f_s \in \mathcal{F}_{loc}$ **do**
      send $\mu^{\{\nu\}}_{f_s \to \Delta x_s}$, $x_s^{\{\nu\}}$ to incidence $\Delta x_s \in \mathcal{X}$
    end for
    for Each $\Delta x_s \in \mathcal{X}$ **do**
      send $\mu^{\{\nu\}\{\rho=0\}}_{\Delta x_s \to f_i} = \mu^{\{\nu\}}_{f_s \to \Delta x_s}$, $x_s^{\{\nu\}}$ to incidence $f_i \in \mathcal{F}_{id}$
    end for
    for Each $f_i \in \mathcal{F}_{ind}$ **do**
      compute residual $r_i^{\{\nu\}} = z_i - h_i(\mathbf{x}^{\{\nu\}})$
      compute Jacobian elements $C^{\{\nu\}}_{i,\Delta x_p}$; $\Delta x_p \in \mathcal{X}_i$
    end for
    procedure INNER ITERATION LOOP $\rho = 1, 2, \ldots$
      while stopping criterion for the inner loop is not met **do**
        for Each $f_i \in \mathcal{F}_{ind}$ **do**
          Compute $\mu^{\{\rho\}}_{f_i \to \Delta x_s}$ using (44)*
        end for
        for Each $\Delta x_s \in \mathcal{X}$ **do**
          Compute $\mu^{\{\rho\}}_{\Delta x_s \to f_i}$ using (42)
        end for
      end while
    end procedure
    for Each $\Delta x_s \in \mathcal{X}$ **do**
      compute $\Delta\hat{x}_s^{\{\nu\}}$ using (47)
      update $x_s^{\{\nu+1\}} = x_s^{\{\nu\}} + \Delta\hat{x}_s^{\{\nu\}}$
    end for
  end while
end procedure
*Incomming messages are obtained in previous iteration $\rho - 1$

The coefficients $C_{\Delta x_p}$, $\Delta x_p \in \mathcal{X}_i$, are Jacobian elements of the measurement function (see Appendix A and B for details) associated with the factor node f_i:

$$C_{\Delta x_p} = \frac{\partial h(x_s, x_l, \ldots, x_L)}{\partial x_p}. \tag{45}$$

Marginal inference: It can be shown that the marginal of the state variable Δx_s, according to (4), is represented by the Gaussian function:

$$p(\Delta x_s) \propto \mathcal{N}(\Delta\hat{x}_s|\Delta x_s, \sigma^2_{\Delta x_s}), \tag{46}$$

with mean $\Delta\hat{x}_s$ which represents the estimated value of the state variable increment Δx_s and variance $\sigma^2_{\Delta x_s}$:

$$\Delta\hat{x}_s = \left(\sum_{f_c \in \mathcal{F}_s} \frac{r_{f_c \to \Delta x_s}}{\sigma^2_{f_c \to \Delta x_s}} \right) \sigma^2_{\Delta x_s} \tag{47a}$$

$$\frac{1}{\sigma^2_{\Delta x_s}} = \sum_{f_c \in \mathcal{F}_s} \frac{1}{\sigma^2_{f_c \to \Delta x_s}}. \quad (47b)$$

To summarize, the MAP sub-problem defined in (40a) can be efficiently solved using (42), (44) and (47).

C. Iterative GN-BP algorithm

Different types of factor nodes and the message-passing schedule presented in Section IV-A will be used to introduce the GN-BP algorithm.

The slack factor node is specified as a node where the voltage angle has a given value, therefore, the residual of the state variable is equal to zero, and the variance approaches to zero. Residuals of initialization and virtual factor nodes approaches to zero, where the variance approaches to infinite. It is important to emphasize that local factor nodes send messages represented by a triplet: mean (residual), variance and state variable (see Appendix C for details).

The GN-BP algorithm is presented in Algorithm 2. The inner iteration loop represents the main routine of algorithm which involves messages inference.

VI. Numerical Results

In this section, we evaluate the performance of the proposed AC BP-based algorithms and compare them to the performance of the Gauss-Newton method (a centralized SE algorithm). More precisely, in the first part, we use the IEEE 14 bus test case to provide a detailed comparison between the accuracy and convergence behavior of the AC-BP and the GN-BP algorithms. In the second part, due to favorable performance of the GN-BP algorithm, we provide an in-depth performance evaluation of this algorithm using the IEEE 14, IEEE 30 and IEEE 118 bus test cases.

A. Simulation setup

For each simulation scenario, we start by a given IEEE bus test case and apply the AC power flow analysis to generate the exact solution for currents, voltages and powers across the network. Further, we corrupt the exact solution by the additive white Gaussian noise of variance σ^2. Finally, we observe the set of measurements that contain active and reactive power flows, active and reactive power injections, bus voltage magnitudes and bus voltage angles. The set of measurements is selected in such a way that the system is observable.

To apply BP-based algorithms, we convert the above scenario into the corresponding factor graph. We run the AC-BP and GN-BP over the factor graph. Note that, to initialize both the BP-based algorithms and the Gauss-Newton method, we use the "flat start"[3] ($V_i = 1$, $\theta_i = 0$, $i = 1, \ldots, N$).

[3]Usually, IEEE bus test cases include in-phase transformers with zero series resistances. Consequently, the "flat start" will cause undefined messages due to the corresponding Jacobian elements being equal to zero. This problem can be alleviated by initializing bus voltage angles with a small random perturbation at transformers' buses.

The proposed algorithms are evaluated and compared using the weighted residual sum of squares (WRSS):

$$\mathrm{WRSS} = \sum_{i=1}^{k} \frac{[z_i - h_i(\mathbf{x})]^2}{\sigma_i^2}. \quad (48)$$

Note that the WRSS is the value of the objective function of the optimization problem (10) we are solving, thus it provides a suitable metric for the accuracy of different algorithms. Besides WRSS, we also use the mean absolute difference (MAD) between the state variables in two consecutive iterations:

$$\mathrm{MAD} = \frac{1}{n}\sum_{i=1}^{n} |\Delta x_i|. \quad (49)$$

The MAD value represents average component-wise shift of the state estimate over the iterations, thus it may be used to quantify the rate of convergence.

In order to present average performance results, we use box plots in which we: i) set the minimum and the maximum value to 0% and 90% of the obtained simulation results, ii) the box is defined by the first and the third quartile, iii) the middle line is the median value, and iv) the results above the maximum value are represented as outliers.

B. Convergence

The set of measurements defines the topology of the factor graph, and for almost all placements of measurement devices of interest, the corresponding factor graph has loops. It is well known that, in general, loopy BP does not converge to correct marginals; e.g., specific inputs may lead to an oscillatory behaviour of messages [36]. Based on extensive numerical studies, we presented in [37] a heuristic solution to improve the convergence of the BP algorithm:

$$\mu^{\rho}_{f\to x} = [1-\delta(p)]\cdot \mu^{\rho}_{f\to x} + \delta(p)\cdot[\alpha_1 \cdot \mu^{\rho-1}_{f\to x} + \alpha_2 \cdot \mu^{\rho}_{f\to x}], \quad (50)$$

where $\delta(p) \in \{0,1\}$ is a Bernoulli random variable with probability p, independently sampled for each message $\mu^{\rho}_{f\to x}$, while α_1 and α_2 are weighting coefficients ($\alpha_1 + \alpha_2 = 1$). As detailed in Section IV-D, we modify updates of selected factor to variable node messages in every iteration by combining them with their values from the previous iteration using convergence parameters p and α_1.

C. Performance Evaluation of AC-BP and GN-BP

The IEEE 14 bus test case with fixed measurement configuration containing 61 measurement devices, as shown in Fig. 7, is used to compare performance of the BP-based SE algorithms. For each value of noise variance $\sigma^2 = \{\sigma_1^2, \sigma_2^2, \sigma_3^2, \sigma_4^2\} = \{0.00001^2, 0.0001^2, 0.001^2, 0.01^2\}$ [p.u.], using Monte Carlo approach, we generate 1000 random sets of measurement values and feed them to the proposed BP-based SE algorithms.

Initially, convergence parameters for BP-based algorithms are set to $p = 0.6$ and $\alpha_1 = 0.5$. The GN-BP is configured so that, for every outer iteration ν, the number of inner

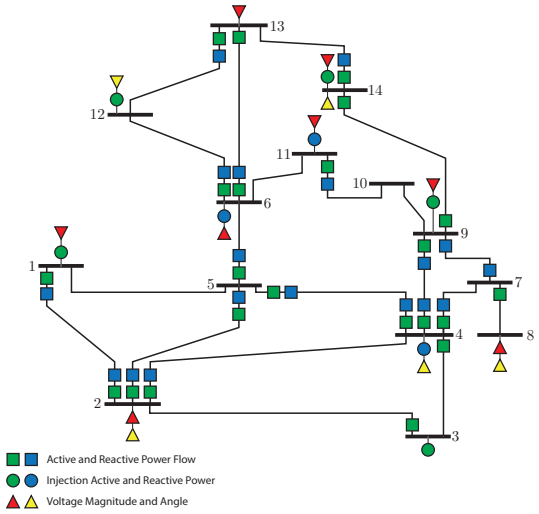

Fig. 7. The IEEE 14 bus test case with given measurement configuration.

iterations is defined as $\tau(\nu) = \nu^q$, where q is the inner iteration exponent, which we set to $q = 4$ [38][4].

We evaluate the performance of the BP-based algorithms using WRSS, normalized by $\mathrm{WRSS}_{\mathrm{wls}}$ of the centralized SE obtained using the Gauss-Newton method after 12 iterations (which we adopt as a normalization constant). Using this normalization, we essentially compare accuracy of BP-based algorithms to the accuracy of the centralized SE.

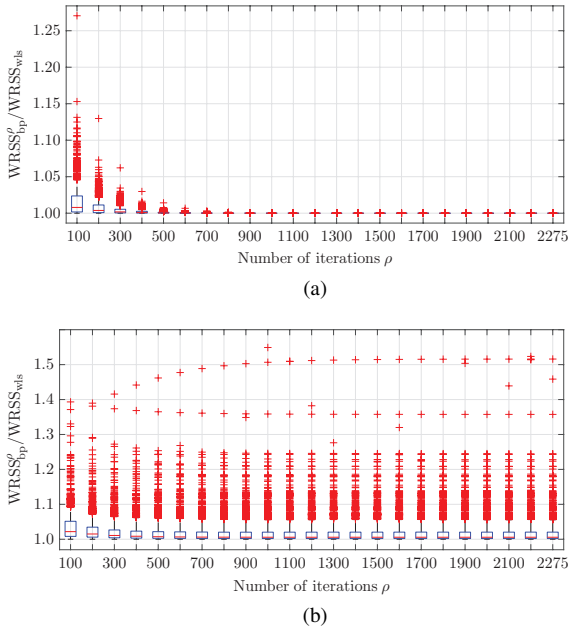

Fig. 8. The AC-BP normalized WRSS (i.e., $\mathrm{WRSS}^{\rho}_{\mathrm{bp}}/\mathrm{WRSS}_{\mathrm{wls}}$) for the low noise level σ_1^2 (subfigure a) and the high noise level σ_4^2 (subfigure b).

Fig. 8 shows the weighted residual sum of squares of the AC-BP $\mathrm{WRSS}^{\rho}_{\mathrm{bp}}$ over the iterations ρ, normalized by $\mathrm{WRSS}_{\mathrm{wls}}$ (i.e., $\mathrm{WRSS}^{\rho}_{\mathrm{bp}}/\mathrm{WRSS}_{\mathrm{wls}}$). We observe that the AC-BP converges for both the low and the high noise level, however, for the high noise level, the solution of the AC-BP algorithm does not correspond to the solution of the centralized SE. This is excepted, as the noise variance increases, the accuracy of Gaussian approximation of the BP messages is decreasing, which affects the accuracy of the AC-BP solution.

Fig. 9 shows $\mathrm{WRSS}^{\nu}_{\mathrm{bp}}/\mathrm{WRSS}_{\mathrm{wls}}$ of the GN-BP over the outer iterations ν. As shown, the GN-BP algorithm converges to the solution of the centralized SE for both the low and the high noise level.

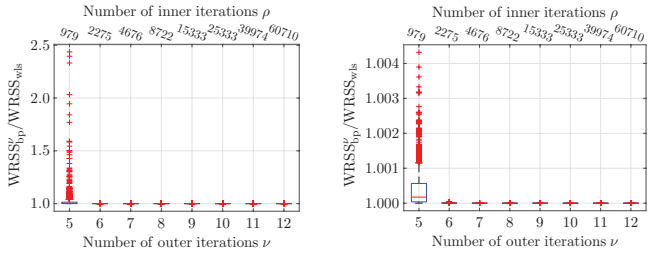

Fig. 9. The GN-BP normalized WRSS (i.e., $\mathrm{WRSS}^{\nu}_{\mathrm{bp}}/\mathrm{WRSS}_{\mathrm{wls}}$) for the low noise level σ_1^2 (subfigure a) and the high noise level σ_4^2 (subfigure b).

To compare BP-based algorithms, we consider $\mathrm{WRSS}_{\mathrm{bp}}$ of the BP-based algorithms after the same total number of iterations. More precisely, the AC-BP algorithm is terminated after $\rho = 2275$ iterations, while the GN-BP is terminated after $\nu = 5$ outer iterations, which corresponds exactly to the total of 2275 inner iterations. Fig. 10 demonstrates that, for the low noise level, the AC-BP converges faster then the GN-BP. However, as the noise level increases, the GN-BP convergence performance significantly outperforms the one of the AC-BP.

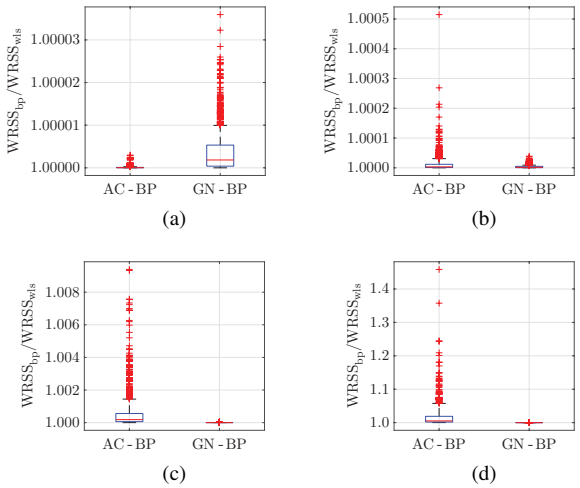

Fig. 10. The normalized WRSS for the AC-BP and GN-BP after 2275 iteration for variances σ_1^2 (subfigure a), σ_2^2 (subfigure b), σ_3^2 (subfigure c) and σ_4^2 (subfigure d).

To summarize, the GN-BP is able to reach the same solution as the centralized SE, while the AC-BP generally does not achieve it for higher noise levels. In addition, in terms of implementation, the AC-BP suffers two drawbacks

[4]Note that in Section IV-D and IV-E we perform detailed performance analysis as a function of convergence parameters and the number of inner iterations.

as compared to the GN-BP: i) the AC-BP messages have considerably more complicated form, and ii) the AC-BP requires prior knowledge (e.g., historical data). Consequently, in the remaining part of this section, we focus on the performance of the GN-BP.

D. Selection of Convergence Parameters

In the following, we analyze the GN-BP convergence performance in order to select appropriate values for convergence parameters p and α_1 introduced in equation (50). Unlike in the previous subsection where a fixed measurement configuration is applied, in this subsection, we generate 1000 random measurement configurations with the number of measurements equal triple the size of the number of state variables (i.e., the redundancy equals to 3). More precisely, from the set of all possible measurements that contains active and reactive power flow measurements located on both side of branches, active and reactive power injection, and voltage magnitude and angle measurements located at each bus, we select a sample uniformly at random according to the predefined redundancy. The set of measurement values are corrupted by additive noise of both the low noise level σ_1^2 and the high noise level σ_4^2. The number of inner iterations is the same as in Section IV-C.

In our simulations, we record the number of non-converging simulations and evaluate the MAD value, both of which will depend on the convergence parameters p and α_1. Informally, the probability p defines a fraction of factor node to variable node messages from a current iteration that are combined with the corresponding messages from a previous iteration. The weighting coefficient α_1 define the ratio that determines how messages from a current and previous iteration are combined. For example, $p = 0.2$ specifies that 20% of messages from a current iteration will be combined with their values in a previous iteration step, while 80% of messages are keeping the values calculated in a current iteration. Furthermore, if $\alpha_1 = 0.1$, then for the 20% of messages, the new value is obtained as a linear combination of the values calculated in the current and the previous iteration with coefficients 0.1 and 0.9, respectively. In the following, we numerically investigate the convergence parameter pairs that lead to acceptable trade-off between the number of non-converging simulations and the rate of convergence.

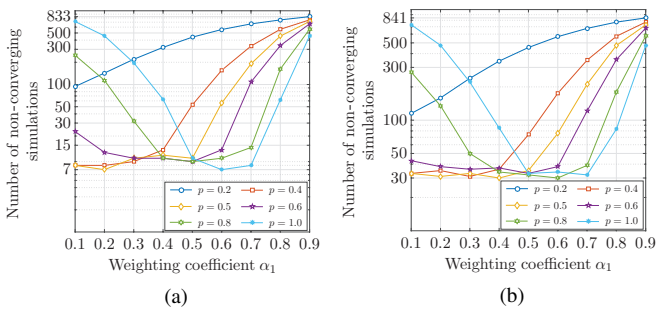

Fig. 11. The number of non-converging simulations (out of 1000 simulations in total) for the low noise level σ_1^2 (subfigure a) and the high noise level σ_4^2 (subfigure b).

Fig. 11 shows the number of non-converging simulations for low noise level σ_1^2 and high noise level σ_4^2 as a function of convergence parameters p and α_1. In general, for the selection of p and α_1 for which only a small fraction of messages are combined with their values in the previous iteration, and that is the case for p close to zero or α_1 close to one, we observe a large number of non-converging simulations. This clearly demonstrates the necessity of using (50) to "slow down" the BP progress, thus increasing the algorithm stability and providing improved convergence.

For a fixed value of α_1, we investigate the convergence rate of GN-BP for different values of p. We expect that, for any selected α_1, the GN-BP will converge faster for smaller values of p, as lower p leads to a reduced "slow down" effect. For example, Fig. 12 shows median MAD values for $\alpha_1 = 0.5$ over the range of p values (where the median is calculated over convergent simulation outcomes only). Figure clearly shows that lower p leads to faster convergence. However, one needs to be careful with selection of p in order to avoid the combinations of p and α_1 that lead to large number of non-converging outcomes.

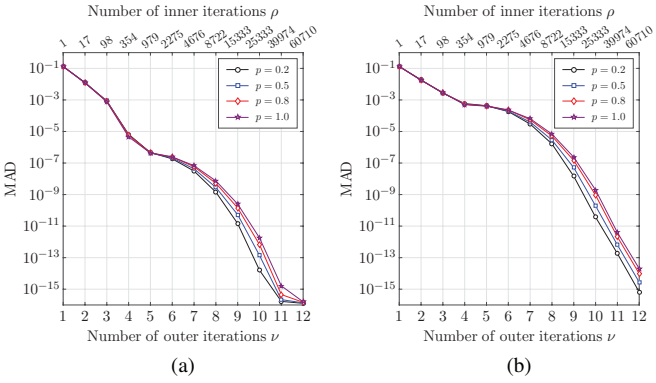

Fig. 12. The median MAD values for $\alpha_1 = 0.5$ over the range of p values for the low noise level σ_1^2 (subfigure a) and the high noise level σ_4^2 (subfigure b).

To select convergence parameters, we observed the median MAD values and the number of non-converging simulations. Table I lists the p and α_1 pairs that demonstrate good performance of both metrics of interest. From the table, we can select e.g., $p = 0.4$ and $\alpha_1 = 0.3$, to achieve good balance between the number of non-converging simulations and the convergence rate.

There are two main causes of non-converging behavior. The main cause is that the number of inner iterations in each outer iteration follows the exponential rule ($\tau = \nu^q$). In general, the GN-BP performs very well with such exponential increase of inner iterations, however, it suffers from insufficient number of inner iterations in the first few outer iterations. Our experiments show that increasing the number of inner iteration only in the first few outer iterations can dramatically reduce the number of non-converging simulations (see the following subsection). The second cause is a combination of "weakly" connected variable nodes and measurements, especially if those nodes represent the buses incident to transformers. In that case, to prevent the

TABLE I
CONVERGENCE PERFORMANCES

Convergence parameters		Median MAD values per iteration (i.e. 7,8,9) Variance σ_1^2			Variance σ_2^2			Number of non-converging simulations	
		7	8	9	7	8	9		
p	α_1	$[10^{-8}]$	$[10^{-9}]$	$[10^{-11}]$	$[10^{-5}]$	$[10^{-6}]$	$[10^{-8}]$	σ_1^2	σ_2^2
0.4	0.1	5.547	5.123	9.942	5.402	4.776	10.411	8	33
0.4	0.2	5.218	4.206	9.427	4.848	3.851	8.775	8	35
0.4	0.3	4.522	3.271	6.697	4.663	3.134	6.593	9	31
0.5	0.2	5.929	5.340	13.782	5.634	5.177	14.042	7	31
0.5	0.3	5.351	4.543	10.061	5.160	4.847	9.514	10	33
0.5	0.4	4.928	3.754	7.316	4.826	3.605	8.060	11	30
0.5	0.5	4.264	2.835	5.309	3.971	2.887	5.096	10	35
0.6	0.5	4.762	4.034	7.354	4.528	3.179	6.902	9	33
0.8	0.5	5.850	5.179	14.215	5.503	5.140	14.454	9	32
0.8	0.6	4.887	3.823	8.595	4.644	3.948	8.800	10	30
1.0	0.6	5.590	5.231	13.882	5.456	4.963	13.086	7	34
1.0	0.7	4.593	3.638	7.097	4.500	3.613	7.084	8	32

non-converging behavior, it is sufficient to connect virtual factor nodes to those variable nodes. Therefore, essentially we can remove the effects of non-converging causes and make the GN-BP algorithm fully reliable.

E. Design of inner iteration schemes

In order to reduce the number of non-converging simulations due to an insufficient number of inner iterations, in this section we test the GN-BP convergence performance with different inner iteration schemes. The convergence parameters are set to $p = 0.4$ and $\alpha_1 = 0.3$. As a reference point, the MAD values of the centralized SE for variances σ_1^2 and σ_4^2 are shown in Fig. 13.

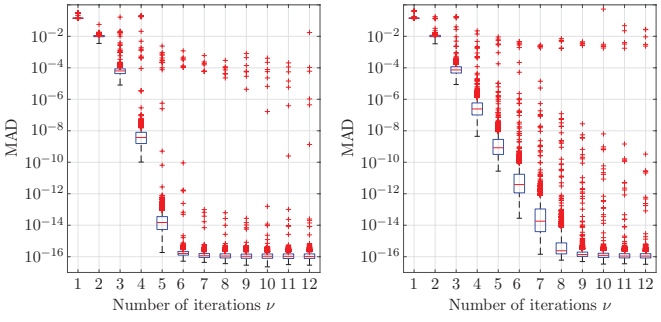

Fig. 13. The MAD values of the centralized SE for the low noise level σ_1^2 (subfigure a) and high noise level σ_4^2 (subfigure b).

For comparison, the MAD values of the GN-BP with the exponential inner iteration scheme ($\tau(\nu) = \nu^q$, $q = 4$) is shown in Fig. 14. Note that the GN-BP exhibits comparable convergence performance to the centralized SE algorithm. Note also that it is difficult to directly compare the two, due to a large difference in computational loads of a single (outer) iteration. For example, the complexity of a single iteration remains constant but significant (due to matrix inversion) over iterations for the centralized SE algorithm, while it gradually increases for the GN-BP starting from an extremely low complexity at initial outer iterations.

In the following, we define an alternative accuracy-based inner iteration scheme. Namely, instead of prescribing the

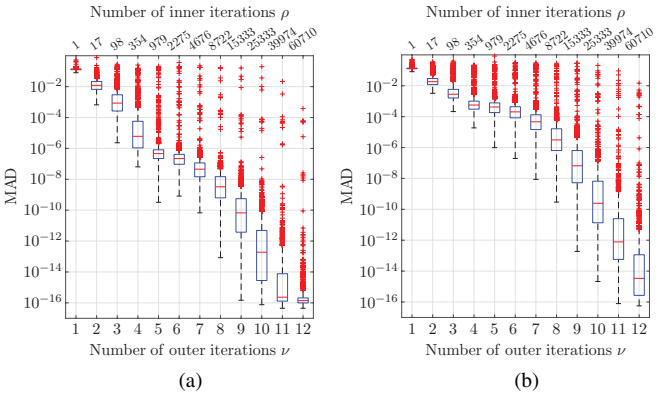

Fig. 14. The MAD values of the GN-BP with the exponential inner iteration scheme for the low noise level σ_1^2 (subfigure a) and high noise level σ_4^2 (subfigure b).

number of inner iterations in advance, we let the number of inner iterations evolve until a certain accuracy-based criterion is met. More precisely, the algorithm in the inner iteration loop is running until the following convergence criterion is reached:

$$|\mathbf{r}_{f\to\Delta x}^{\nu,\rho} - \mathbf{r}_{f\to\Delta x}^{\nu,\rho-1}| < \epsilon(\nu), \tag{51}$$

where $\mathbf{r}_{f\to\Delta x}$ represents the vector of mean-value messages from factor nodes to variable nodes, and $\epsilon(\nu)$ is the threshold at iteration ν. Note that, due the fact that the BP is a distributed algorithm, imposing this condition in real systems would require additional communication overhead.

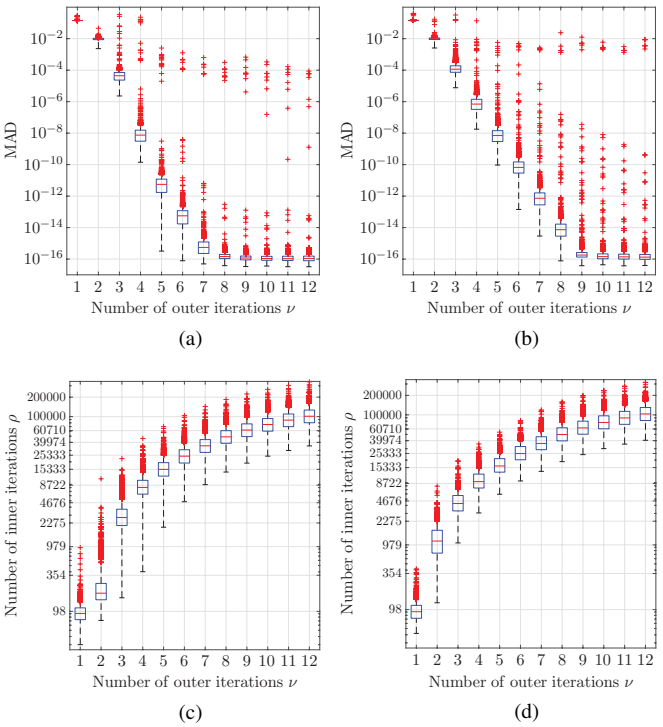

Fig. 15. The MAD values and the number of inner iterations for the low noise level σ_1^2 (subfigure a and subfigure c) and the high noise level σ_4^2 (subfigure b and subfigure d) of the GN-BP with the threshold $\epsilon(\nu) = [10^{-2}, 10^{-4}, \ldots, 10^{-16}, \ldots, 10^{-16}]$.

Fig. 15 shows MAD values and the total number of inner iterations for the threshold $\epsilon(\nu) = [10^{-2}, 10^{-4}, \ldots, 10^{-16}, \ldots, 10^{-16}]$, where the number of outer iterations is $\nu = 1, \ldots, 12$. Comparing the results in Fig. 13 and Fig. 15, we observe that the convergence behavior of the GN-BP with accuracy-based inner iteration scheme is similar to the centralized SE. If compared to the GN-BP with exponential inner iteration scheme, we note that for the low noise level σ_1^2 and for lower MAD values (e.g. $\sim 10^{-4}$) the exponential scheme results in better performance. For all other cases, the the GN-BP with accuracy-based scheme provides a similar or better performance. Note that, the proposed accuracy-based inner iteration scheme dramatically reduces the number of non-converging simulations (i.e. two for the low noise level and four for the high noise level).

Fig. 16 illustrates the accuracy-based scheme performance for $\epsilon(\nu) = [10^{-3}, 10^{-6}, \ldots, 10^{-15}, 10^{-16}, \ldots, 10^{-16}]$. Comparing the results with the centralized SE (Fig. 13), we note that the GN-BP has almost identical convergence rate.

To summarize, we have demonstrated that by using different inner iteration schemes, one can influence and control the trade-off between the GN-BP convergence rate and the total number of inner iterations.

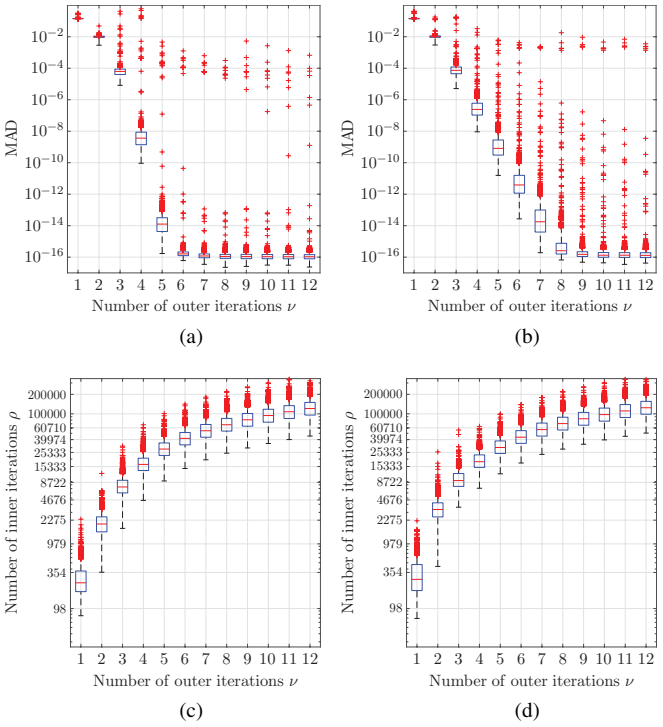

Fig. 16. The MAD values and the number of inner iterations for the low noise level σ_1^2 (subfigure a and subfigure c) and the high noise level σ_4^2 (subfigure b and subfigure d) of the GN-BP with threshold $\epsilon(\nu) = [10^{-3}, 10^{-6}, \ldots, 10^{-15}, 10^{-16}, \ldots, 10^{-16}]$.

F. Scalability of the GN-BP algorithm

To demonstrate scalability of the GN-BP algorithm, we provide MAD values for the IEEE 30 and IEEE 118 bus test case. As before, we generate 1000 random measurement configurations with the redundancy equal to 3. The set of measurement values are corrupted by additive noise of both the low noise level σ_1^2 and the high noise level σ_4^2. The convergence parameters are set to $p = 0.4$ and $\alpha_1 = 0.3$ and we use the exponential inner iteration scheme. From Fig. 17

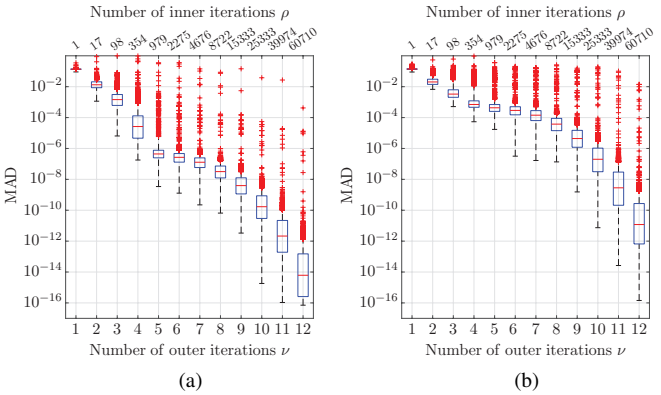

Fig. 17. The MAD values of the GN-BP for the IEEE 30 bus test case with the exponential inner iteration scheme ($\tau(\nu) = \nu^q$) for the low noise level σ_1^2 (subfigure a) and high noise level σ_4^2 (subfigure b).

and Fig. 18, we note that the GN-BP converges, however, the rate of convergence slightly decreases as the size of the system increases. As described in the previous subsection, one can use different inner iteration schemes to fine-tune the rate of convergence.

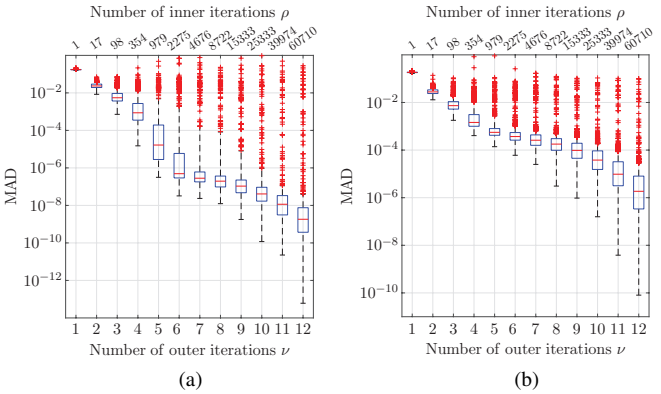

Fig. 18. The MAD values of the GN-BP for the IEEE 118 bus test case with the exponential inner iteration scheme ($\tau(\nu) = \nu^q$) for the low noise level σ_1^2 (subfigure a) and high noise level σ_4^2 (subfigure b).

G. Complexity of the GN-BP algorithm

Let us first consider the complexity of the centralized SE based on the Gauss-Newton method. For n state variables and k measurements, each iteration of the centralized SE involves a constant number of matrix multiplications and a matrix inversion whose complexity is of the order of $\mathcal{O}(kn^2)$ and $\mathcal{O}(n^3)$, respectively. Due to the fact that k is proportional to n for observable systems, and that the centralized SE takes constant number of iterations to converge, the overall complexity of the centralized SE scales as $\mathcal{O}(n^3)$. However, this can be reduced by employing matrix inversion techniques that exploit the sparsity of

involved matrices. The resulting sparsity-aware centralized SE methods operate with complexity that scales as $O(n^2)$ [39], [40].

The complexity of BP depends on the sparsity of the underlying factor graph, as the computational effort per iteration is proportional to the number of edges in the factor graph. For each of the k measurements, the degree (the number of incident edges) of the corresponding factor node is limited by a (typically small) constant. Indeed, for any type of measurements, the corresponding measurement function depends only on a few state variables corresponding to the buses in the local neighbourhood of the bus/branch where the measurement is taken. Thus as n and k grow large, the number of edges in the factor graph scales as $\mathcal{O}(n)$, which corresponds to the computation complexity of BP *per iteration*. The scaling of the number of BP iterations ρ as n grows large is a challenging problem. Based on discussion in [41] for full matrices, the number of iterations is likely to scale with condition number of the underlying matrix, which for well-conditioned matrices may scale as low as $O(1)$. However, we leave the more detailed analysis on the scaling of the number of GN-BP iterations for our future work.

To summarize, BP approach builds upon the factor graph structure that directly exploits the underlying system sparsity, thus achieving minimal complexity of $\mathcal{O}(n)$ per iteration, while the scaling of the number of iterations needs further study. In contrast to the optimized centralized methods whose complexity scales as $\mathcal{O}(n^2)$, the BP method can be flexibly distributed by arbitrarily segmenting the underlying factor graph into disjoint areas. In the extreme case of the fully-distributed BP algorithm (that we focus on in this paper), each factor graph node operates locally and independently. Thus, the SE problem is distributed across $\mathcal{O}(n)$ nodes, and if implemented to run in parallel, can be $\mathcal{O}(n)$ times faster than the centralized solution. In addition, for fully-distributed BP, none of the nodes need to store the system-level matrices (whose storage-size typically scales as $\mathcal{O}(n^2)$), and storing only constant-size set of local parameters is sufficient.

VII. Conclusions

In this paper, we presented an in-depth study of the applications of factor graphs and the BP algorithm to the SE problem in power systems. We provided detailed derivation and performance analysis of the two fully-distributed BP-based SE algorithms: the AC-BP and the GN-BP algorithm. The central point of our study was the GN-BP algorithm, which is shown to represent a BP-based implementation of the iterative Gauss-Newton method, achieving the same accuracy as the centralized SE. In a thorough numerical study, we have shown how to fine-tune the GN-BP implementation and balance between the accuracy and the convergence rate. In our future work, we will investigate further advantages brought in by addressing the SE problem using the BP framework, such as extensions to asynchronous BP in dynamic state estimation, detailed analysis of BP-based methods in multi-area state estimation, learning graphical model parameters from observed data, and many others.

Appendix A
Jacobian elements

The Jacobian elements corresponding to non-linear measurement functions (11) - (13) are described below.

- The Jacobian expressions corresponding to $h_{P_{ij}}(\cdot)$ are as follows:

$$\frac{\partial h_{P_{ij}}(\cdot)}{\partial \theta_i} = V_i V_j (g_{ij}\text{sin}\theta_{ij} - b_{ij}\text{cos}\theta_{ij})$$
$$\frac{\partial h_{P_{ij}}(\cdot)}{\partial \theta_j} = -V_i V_j (g_{ij}\text{sin}\theta_{ij} - b_{ij}\text{cos}\theta_{ij})$$
$$\frac{\partial h_{P_{ij}}(\cdot)}{\partial V_i} = -V_j (g_{ij}\text{cos}\theta_{ij} + b_{ij}\text{sin}\theta_{ij}) + 2V_i(g_{ij} + g_{si})$$
$$\frac{\partial h_{P_{ij}}(\cdot)}{\partial V_j} = -V_i (g_{ij}\text{cos}\theta_{ij} + b_{ij}\text{sin}\theta_{ij}).$$

- The Jacobian expressions corresponding to $h_{Q_{ij}}(\cdot)$ are as follows:

$$\frac{\partial h_{Q_{ij}}(\cdot)}{\partial \theta_i} = -V_i V_j (g_{ij}\text{cos}\theta_{ij} + b_{ij}\text{sin}\theta_{ij})$$
$$\frac{\partial h_{Q_{ij}}(\cdot)}{\partial \theta_j} = V_i V_j (g_{ij}\text{cos}\theta_{ij} + b_{ij}\text{sin}\theta_{ij})$$
$$\frac{\partial h_{Q_{ij}}(\cdot)}{\partial V_i} = -V_j (g_{ij}\text{sin}\theta_{ij} - b_{ij}\text{cos}\theta_{ij}) - 2V_i(b_{ij} + b_{si})$$
$$\frac{\partial h_{Q_{ij}}(\cdot)}{\partial V_j} = -V_i (g_{ij}\text{sin}\theta_{ij} - b_{ij}\text{cos}\theta_{ij}).$$

- The Jacobian expressions corresponding to current magnitude measurement function $h_{I_{ij}}(\cdot)$ are as follows:

$$\frac{\partial h_{I_{ij}}(\cdot)}{\partial \theta_i} = \frac{V_i V_j (D_c \cos\theta_{ij} + C_c \sin\theta_{ij})}{I_{ij}}$$
$$\frac{\partial h_{I_{ij}}(\cdot)}{\partial \theta_j} = -\frac{V_i V_j (D_c \cos\theta_{ij} + C_c \sin\theta_{ij})}{I_{ij}}$$
$$\frac{\partial h_{I_{ij}}(\cdot)}{\partial V_i} = \frac{V_j (D_c \sin\theta_{ij} - C_c \cos\theta_{ij}) + A_c V_i}{I_{ij}}$$
$$\frac{\partial h_{I_{ij}}(\cdot)}{\partial V_j} = \frac{V_i (D_c \sin\theta_{ij} - C_c \cos\theta_{ij}) + B_c V_j}{I_{ij}}.$$

- The Jacobian expressions corresponding to $h_{P_i}(\cdot)$ are:

$$\frac{\partial h_{P_i}(\cdot)}{\partial \theta_i} = V_i \sum_{j \in \mathcal{H}_i \setminus i} V_j (-G_{ij}\text{sin}\theta_{ij} + B_{ij}\text{cos}\theta_{ij})$$
$$\frac{\partial h_{P_i}(\cdot)}{\partial \theta_j} = V_i V_j (G_{ij}\text{sin}\theta_{ij} - B_{ij}\text{cos}\theta_{ij})$$
$$\frac{\partial h_{P_i}(\cdot)}{\partial V_i} = \sum_{j \in \mathcal{H}_i \setminus i} V_j (G_{ij}\text{cos}\theta_{ij} + B_{ij}\text{sin}\theta_{ij}) + 2V_i G_{ii}$$
$$\frac{\partial h_{P_i}(\cdot)}{\partial V_j} = V_i (G_{ij}\text{cos}\theta_{ij} + B_{ij}\text{sin}\theta_{ij}),$$

where $\mathcal{H}_i \setminus i$ is the set of buses incident to the bus i.

• The Jacobian expressions corresponding to $h_{Q_i}(\cdot)$ are:

$$\frac{\partial h_{Q_i}(\cdot)}{\partial \theta_i} = V_i \sum_{j\in\mathcal{H}_i\setminus i} V_j(G_{ij}\text{cos}\theta_{ij} + B_{ij}\text{sin}\theta_{ij})$$
$$\frac{\partial h_{Q_i}(\cdot)}{\partial \theta_j} = V_iV_j(-G_{ij}\text{cos}\theta_{ij} - B_{ij}\text{sin}\theta_{ij})$$
$$\frac{\partial h_{Q_i}(\cdot)}{\partial V_i} = \sum_{j\in\mathcal{H}_i\setminus i} V_j(G_{ij}\text{sni}\theta_{ij} - B_{ij}\text{cos}\theta_{ij}) - 2V_iB_{ii}$$
$$\frac{\partial h_{Q_i}(\cdot)}{\partial V_j} = V_i(G_{ij}\text{sin}\theta_{ij} - B_{ij}\text{cos}\theta_{ij}).$$

• The Jacobian expressions corresponding to measurements of voltage magnitude and voltage angle are as follows:

$$\frac{\partial V_i}{\partial V_i} = 1; \quad \frac{\partial \theta_i}{\partial \theta_i} = 1.$$

APPENDIX B
THE AC-BP: MEAN AND VARIANCE OF A MESSAGE FROM A FACTOR NODE TO A VARIABLE NODE

Here we present an example of evaluation of the message from a factor node to a variable node for the AC-BP algorithm. We consider a simple model containing buses i and j, with the active power flow measurement $M_i \equiv M_{P_{ij}}$ at the branch (i,j). The mean z_i, variance σ_i^2 and the measurement function $h_i(\theta_i, V_i, \theta_j, V_j)$ defined as (11a) is associated with the active power flow measurement M_i. The corresponding factor graph is shown in Fig. 19.

Further, all incoming messages from variable nodes to the factor node f_i have Gaussian form. Therefore, these messages, denoted as $\mu_{\theta_i\to f_i}(\theta_i)$, $\mu_{V_i\to f_i}(V_i)$, $\mu_{\theta_j\to f_i}(\theta_j)$ and $\mu_{V_j\to f_i}(V_j)$, are represented by their mean-variance pair $(z_{\theta_i\to f_i}, \sigma^2_{\theta_i\to f_i})$, $(z_{V_i\to f_i}, \sigma^2_{V_i\to f_i})$, $(z_{\theta_j\to f_i}, \sigma^2_{\theta_j\to f_i})$ and $(z_{V_j\to f_i}, \sigma^2_{V_j\to f_i})$, respectively (Fig. 19a - Fig. 19d).

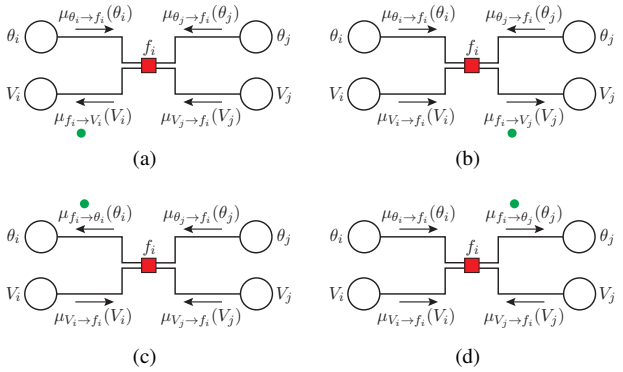

Fig. 19. Messages from from factor node f_i to variable nodes: V_i (subfigure a), V_j (subfigure b), θ_i (subfigure c) and θ_j (subfigure d).

According to assumption (see Section IV), the messages from the factor node f_i to variable nodes have Gaussian form: $\mu_{f_i\to V_i}(V_i)$, $\mu_{f_i\to V_j}(V_j)$, $\mu_{f_i\to\theta_i}(\theta_i)$ and $\mu_{f_i\to\theta_j}(\theta_j)$ with their mean-variance pair $(z_{f_i\to V_i}, \sigma^2_{f_i\to V_i})$, $(z_{f_i\to V_j}, \sigma^2_{f_i\to V_j})$, $(z_{f_i\to\theta_i}, \sigma^2_{f_i\to\theta_i})$ and $(z_{f_i\to\theta_j}, \sigma^2_{f_i\to\theta_j})$. In the following, we consider calculation of each of these messages.

• The message $\mu_{f_i\to V_i}$ (Fig. 19a): Let us first consider the mean $z_{f_i\to V_i}$. The equation (23) for the active power flow measurement boils down to (26b):

$$a\mathbb{E}[V_i^2|\mathbf{x}_b = \mathbf{z}_{\mathbf{x}_b\to f_i}] + b\mathbb{E}[V_i|\mathbf{x}_b = \mathbf{z}_{\mathbf{x}_b\to f_i}] + c = 0,$$

where: $\mathbf{x}_b = (\theta_i, \theta_j, V_j)$ and $\mathbf{z}_{\mathbf{x}_b\to f_i} = (z_{\theta_i\to f_i}, z_{\theta_j\to f_i}, z_{V_j\to f_i})$, with coefficients:

$$a = g_{ij} + g_{si}$$
$$b = -z_{V_j\to f_i}(g_{ij}\cos z_{\theta_{ij}\to f_i} + b_{ij}\sin z_{\theta_{ij}\to f_i})$$
$$c = -z_i,$$

where $z_{\theta_{ij}\to f_i}$ is determined as $z_{\theta_i\to f_i} - z_{\theta_j\to f_i}$. Due the fact that the conditional expected value $\mathbb{E}[V_i|\mathbf{x}_b = \mathbf{z}_{\mathbf{x}_b\to f_i}]$ represents the mean $z_{f_i\to V_i}$, we can write:

$$a(z^2_{f_i\to V_i} + \sigma^2_{f_i\to V_i}) + bz_{f_i\to V_i} + c = 0.$$

The mean $z_{f_i\to V_i}$ follows from the quadratic equation, where we selected a solution using (27).

The variance $\sigma^2_{f_i\to V_i}$ is determined using (28) as:

$$\sigma^2_{f_i\to V_i} = \frac{1}{C^2_{V_i}}(\sigma_i^2 + C^2_{\theta_i}\sigma^2_{\theta_i\to f_i} + C^2_{\theta_j}\sigma^2_{\theta_j\to f_i} + C^2_{V_j}\sigma^2_{V_j\to f_i}),$$

where coefficients are defined according to Jacobian elements of the measurement function $h_i(\cdot)$:

$$C_{\theta_i} = \left.\frac{\partial h_i(V_i,\mathbf{x}_b)}{\partial\theta_i}\right|_{\substack{V_i=z_{f_i\to V_i}\\ \mathbf{x}_b=\mathbf{z}_{\mathbf{x}_b\to f_i}}} \quad C_{\theta_j} = \left.\frac{\partial h_i(V_i,\mathbf{x}_b)}{\partial\theta_j}\right|_{\substack{V_i=z_{f_i\to V_i}\\ \mathbf{x}_b=\mathbf{z}_{\mathbf{x}_b\to f_i}}}$$
$$C_{V_i} = \left.\frac{\partial h_i(V_i,\mathbf{x}_b)}{\partial V_i}\right|_{\substack{V_i=z_{f_i\to V_i}\\ \mathbf{x}_b=\mathbf{z}_{\mathbf{x}_b\to f_i}}} \quad C_{V_j} = \left.\frac{\partial h_i(V_i,\mathbf{x}_b)}{\partial V_j}\right|_{\substack{V_i=z_{f_i\to V_i}\\ \mathbf{x}_b=\mathbf{z}_{\mathbf{x}_b\to f_i}}}$$

• The message $\mu_{f_i\to V_j}$ (Fig. 19b): The mean $z_{f_i\to V_j}$ is defined according to (26a) as:

$$a\mathbb{E}[V_j|\mathbf{x}_b = \mathbf{z}_{\mathbf{x}_b\to f_i}] + b = 0,$$

where: $\mathbf{x}_b = (\theta_i, V_i, \theta_j)$ and $\mathbf{z}_{\mathbf{x}_b\to f_i} = (z_{\theta_i\to f_i}, z_{V_i\to f_i}, z_{\theta_j\to f_i})$, with coefficients:

$$a = z_i - z^2_{V_i\to f_i}(g_{ij} + g_{si})$$
$$b = z_{V_i\to f_i}(g_{ij}\cos z_{\theta_{ij}\to f_i} + b_{ij}\sin z_{\theta_{ij}\to f_i}).$$

Due the fact that the conditional expected value $\mathbb{E}[V_j|\mathbf{x}_b = \mathbf{z}_{\mathbf{x}_b\to f_i}]$ represents the mean $z_{f_i\to V_j}$, we obtain:

$$az_{f_i\to V_j} + b = 0.$$

The variance $\sigma^2_{f_i\to V_j}$ is determined using (28) as:

$$\sigma^2_{f_i\to V_j} = \frac{1}{C^2_{V_j}}(\sigma_i^2 + C^2_{\theta_i}\sigma^2_{\theta_i\to f_i} + C^2_{V_i}\sigma^2_{V_i\to f_i} + C^2_{\theta_j}\sigma^2_{\theta_j\to f_i}),$$

where coefficient are defined according to Jacobian elements of the measurement function $h_i(\cdot)$.

• The messages $\mu_{f_i\to\theta_i}$ and $\mu_{f_i\to\theta_j}$ (Fig. 19c and Fig. 19d): Means $z_{f_i\to\theta_i}$ and $z_{f_i\to\theta_j}$ are defined according to (26c):

$$a\mathbb{E}[\sin^2 x_s|\mathbf{x}_b = \mathbf{z}_{\mathbf{x}_b\to f_i}] + b\mathbb{E}[\sin x_s|\mathbf{x}_b = \mathbf{z}_{\mathbf{x}_b\to f_i}] + c = 0,$$

where: $\mathbf{x}_b = (V_i, \theta_j, V_j)$ and $\mathbf{z}_{\mathbf{x}_b\to f_i} = (z_{V_i\to f_i}, z_{\theta_j\to f_i},$

$z_{V_j \to f_i}$) for the message $\mu_{f_i \to \theta_i}$, $\mathbf{x}_b = (\theta_i, V_i, V_j)$ and $\mathbf{z}_{\mathbf{x}_b \to f_i} = (z_{\theta_i \to f_i}, z_{V_i \to f_i}, z_{V_j \to f_i})$ for the message $\mu_{f_i \to \theta_j}$, and $x_s \in \{\theta_i, \theta_j\}$. Due the fact that the all variables and messages preserve Gaussian distribution, the conditional expectations of sine functions are equal to $\mathbb{E}[\sin^2 x_s | \mathbf{x}_b = \mathbf{z}_{\mathbf{x}_b \to f_i}] = \sin^2 z_{f_i \to x_s}$ and $\mathbb{E}[\sin x_s | \mathbf{x}_b = \mathbf{z}_{\mathbf{x}_b \to f_i}] = \sin z_{f_i \to x_s}$, which allows us to compute the mean:

$$a \sin^2 z_{f_i \to x_s} + b \sin z_{f_i \to x_s} + c = 0.$$

To simplify expressions, we introduce coefficients $a = A^2 + B^2$, $b = -2BC$ and $c = -A^2 + C^2$:

$$\begin{aligned}
A &= g_{ij} \cos z_{\theta_j \to f_i} - b_{ij} \sin z_{\theta_j \to f_i}, && x_s \equiv \theta_i \\
A &= g_{ij} \cos z_{\theta_i \to f_i} + b_{ij} \sin z_{\theta_i \to f_i}, && x_s \equiv \theta_j \\
B &= g_{ij} \sin z_{\theta_j \to f_i} + b_{ij} \cos z_{\theta_j \to f_i}, && x_s \equiv \theta_i \\
B &= g_{ij} \sin z_{\theta_i \to f_i} - b_{ij} \cos z_{\theta_i \to f_i}, && x_s \equiv \theta_i \\
C &= \frac{z^2_{V_i \to f_i}(g_{ij} + g_{si}) - z_i}{z_{V_i \to f_i} z_{V_j \to f_i}}, && x_s \in \{\theta_i, \theta_j\}
\end{aligned}$$

The variance $\sigma^2_{f_i \to \theta_i}$ is determined using (28) as:

$$\sigma^2_{f_i \to \theta_i} = \frac{1}{C^2_{\theta_i}} (\sigma_i^2 + C^2_{V_i} \sigma^2_{V_i \to f_i} + C^2_{\theta_j} \sigma^2_{\theta_j \to f_i} + C^2_{V_j} \sigma^2_{V_j \to f_i}),$$

where coefficients are defined, as above, by calculating Jacobian elements of the measurement function $h_i(\cdot)$.

The variance $\sigma^2_{f_i \to \theta_j}$ is determined according to (28) as:

$$\sigma^2_{f_i \to \theta_j} = \frac{1}{C^2_{\theta_j}} (\sigma_i^2 + C^2_{\theta_i} \sigma^2_{\theta_i \to f_i} + C^2_{V_i} \sigma^2_{V_i \to f_i} + C^2_{V_j} \sigma^2_{V_j \to f_i}),$$

where coefficient follow Jacobian elements of the measurement function $h_{P_i}(\cdot)$.

Using the same methodology, it is possible to define corresponding equations for means and variances for every type of measurement functions.

APPENDIX C
THE GN-BP ALGORITHM: TOY EXAMPLE

An illustrative example presented in Fig. 6a will be used to provide a step-by-step presentation of the proposed algorithm.

Input data for SE from measurement devices are Gaussian-type functions represented by means and variances: $\{z_{V_1}, z_{\theta_2}, z_{\theta_3}, z_{P_{12}}, z_{P_3}\}$ and $\{\sigma^2_{V_1}, \sigma^2_{\theta_2}, \sigma^2_{\theta_3}, \sigma^2_{P_{12}}, \sigma^2_{P_3}\}$.

The corresponding factor graph is given in Fig. 20, where indirect factor nodes (red squares) are $f_{r_{P_{12}}}$ and $f_{r_{P_3}}$, while direct factor nodes (orange squares) are $f_{r_{V_1}}$, $f_{r_{\theta_2}}$ and $f_{r_{\theta_3}}$. The slack factor node $f_{r_{\theta_1}}$ (yellow square) corresponds to the slack or reference bus. The initialization (green square) and virtual (blue square) factor nodes are $f_{r_{V_2}}$ and $f_{r_{V_3}}$, respectively.

Each variable node in the initialization step of the algorithm has the corresponding local factor node. Local factor nodes only send, but do not receive, the messages to the incident variable nodes. Direct and virtual factor nodes always repeat the same message to their corresponding variable nodes through iterations.

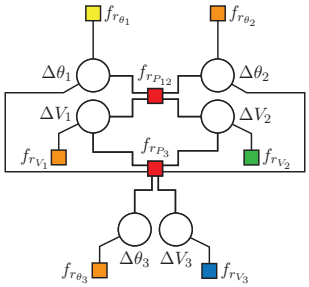

Fig. 20. Factor graph of the bus/branch model with given measurement configuration shown in Fig. 6a.

In the following, for notational convenience, we denote the variance as follows: $\sigma^2 \equiv v$.

Algorithm Initialization

1) The AC SE in electric power systems assumes "flat start" or a priori given values of state variables:
$$\mathbf{x}^{\{\nu=0\}} = [\theta_1\ \theta_2\ \theta_3\ V_1\ V_2\ V_3]^{\{\nu=0\}}.$$
2) The residual of the slack factor node is set to $r_{\theta_1} = 0$ with variance $v_{\theta_1} \to 0$.
3) The value of initialization factor nodes and virtual factor nodes are set to $r_{V_2} \to 0$ and $r_{V_3} \to 0$, with variances $v_{V_2} \to \infty$ and $v_{V_3} \to \infty$.

Iterate - Outer Loop: $\boldsymbol{\nu} = \mathbf{0}, \mathbf{1}, \mathbf{2}, \ldots$; $\boldsymbol{\rho} = \mathbf{0}$

4) Each direct factor node computes residual, e.g.:
$$r^{\{\nu\}}_{V_1} = z_{V_1} - V_1^{\{\nu\}}.$$
5) Local factor nodes send messages represented by a triplet (residual, variance, state variable), to incident variable nodes, e.g.:
$$\begin{aligned}
\mu^{\{\nu\}}_{f_{r_{\theta_1}} \to \Delta\theta_1} &:= \left(r_{\theta_1}, v_{\theta_1}, \theta_1^{\{\nu\}}\right) \\
\mu^{\{\nu\}}_{f_{r_{V_1}} \to \Delta V_1} &:= \left(r^{\{\nu\}}_{V_1}, v_{V_1}, V_1^{\{\nu\}}\right).
\end{aligned}$$
6) Variable nodes forward the incoming messages received from local factor nodes along remaining edges, e.g.:
$$\begin{aligned}
\mu^{\{\nu\}\{\rho\}}_{\Delta\theta_1 \to f_{r_{P_{12}}}} &= \mu^{\{\nu\}}_{f_{r_{\theta_1}} \to \Delta\theta_1} := \left(r^{\{\nu\}}_{\theta_1}, v_{\theta_1}, \theta_1^{\{\nu\}}\right) \\
&:= \left(r^{\{\nu\}\{\rho\}}_{\Delta\theta_1 \to f_{r_{P_{12}}}}, v^{\{\nu\}\{\rho\}}_{\Delta\theta_1 \to f_{r_{P_{12}}}}, \theta_1^{\{\nu\}\{\rho\}}\right) \\
\mu^{\{\nu\}\{\rho\}}_{\Delta\theta_1 \to f_{r_{P_3}}} &= \mu^{\{\nu\}}_{f_{r_{\theta_1}} \to \Delta\theta_1} := \left(r^{\{\nu\}}_{\theta_1}, v_{\theta_1}, \theta_1^{\{\nu\}}\right) \\
&:= \left(r^{\{\nu\}\{\rho\}}_{\Delta\theta_1 \to f_{r_{P_3}}}, v^{\{\nu\}\{\rho\}}_{\Delta\theta_1 \to f_{r_{P_3}}}, \theta_1^{\{\nu\}\{\rho\}}\right).
\end{aligned}$$
7) Indirect factor nodes compute residuals, e.g.:
$$r^{\{\nu\}}_{P_{12}} = z_{P_{12}} - h_{P_{12}}(\theta_1^{\{\nu\}}, \theta_2^{\{\nu\}}, V_1^{\{\nu\}}, V_2^{\{\nu\}}).$$
8) Indirect factor nodes compute appropriate Jacobian elements associated with state variables, e.g.:
$$\begin{aligned}
C^{\{\nu\}}_{P_{12},\Delta\theta_1} &= \frac{\partial h_{P_{12}}(\cdot)}{\partial \theta_1} = V_1^{\{\nu\}} V_2^{\{\nu\}} (g_{12} \sin\theta_{12}^{\{\nu\}} - b_{12} \cos\theta_{12}^{\{\nu\}}) \\
C^{\{\nu\}}_{P_{12},\Delta V_2} &= \frac{\partial h_{P_{12}}(\cdot)}{\partial V_2} = -V_1^{\{\nu\}} (g_{12} \cos\theta_{12}^{\{\nu\}} + b_{12} \sin\theta_{12}^{\{\nu\}}).
\end{aligned}$$

Iterate - Inner Loop: $\boldsymbol{\rho} = \mathbf{1}, \mathbf{2}, \ldots, \boldsymbol{\tau}(\boldsymbol{\nu})$

9) Indirect factor nodes send messages as pairs along incident edges according to (44), e.g.:

$$\mu^{\{\rho\}}_{f_{P_{12}}\to\Delta\theta_2} := \big(r^{\{\rho\}}_{f_{P_{12}}\to\Delta\theta_2}, v^{\{\rho\}}_{f_{P_{12}}\to\Delta\theta_2}\big)$$

$$r^{\{\rho\}}_{f_{r_{P_{12}}}\to\Delta\theta_2} = \frac{1}{C^{\{\nu\}}_{P_{12},\Delta\theta_2}}\Big[r^{\{\nu\}}_{P_{12}} - C^{\{\nu\}}_{P_{12},\Delta\theta_1}\cdot r^{\{\nu\}\{\rho-1\}}_{\Delta\theta_1\to f_{r_{P_{12}}}} - C^{\{\nu\}}_{P_{12},\Delta V_1}\cdot r^{\{\nu\}\{\rho-1\}}_{\Delta V_1\to f_{r_{P_{12}}}} - C^{\{\nu\}}_{P_{12},\Delta V_2}\cdot r^{\{\nu\}\{\rho-1\}}_{\Delta V_2\to f_{r_{P_{12}}}}\Big]$$

$$v^{\{\rho\}}_{f_{r_{P_{12}}}\to\Delta\theta_2} = \frac{1}{(C^{\{\nu\}}_{P_{12},\Delta\theta_2})^2}\Big[v_{P_{12}} + (C^{\{\nu\}}_{P_{12},\Delta\theta_1})^2\cdot v^{\{\nu\}\{\rho-1\}}_{\Delta\theta_1\to f_{r_{P_{12}}}} + (C^{\{\nu\}}_{P_{12},\Delta V_1})^2\cdot v^{\{\nu\}\{\rho-1\}}_{\Delta V_1\to f_{r_{P_{12}}}} + (C^{\{\nu\}}_{P_{12},\Delta V_2})^2\cdot v^{\{\nu\}\{\rho-1\}}_{\Delta V_2\to f_{r_{P_{12}}}}\Big].$$

10) Variable nodes send messages as pairs along incident edges to indirect factor nodes according to (18), e.g.:

$$\mu^{\{\nu\}\{\rho\}}_{\Delta\theta_2\to f_{r_{P_{12}}}} := \big(r^{\{\nu\}\{\rho\}}_{\Delta\theta_2\to f_{r_{P_{12}}}}, v^{\{\nu\}\{\rho\}}_{\Delta\theta_2\to f_{r_{P_{12}}}}\big)$$

$$\frac{1}{v^{\{\nu\}\{\rho\}}_{\Delta\theta_2\to f_{r_{P_{12}}}}} = \frac{1}{v_{\theta_2}} + \frac{1}{v^{\{\rho\}}_{f_{r_{P_3}}\to\Delta\theta_2}}$$

$$r^{\{\nu\}\{\rho\}}_{\Delta\theta_2\to f_{r_{P_{12}}}} = \left(\frac{r^{\{\nu\}}_{\theta_2}}{v_{\theta_2}} + \frac{r^{\{\rho\}}_{f_{r_{P_3}}\to\Delta\theta_2}}{v^{\{\rho\}}_{f_{r_{P_3}}\to\Delta\theta_2}}\right) v^{\{\rho\}}_{\Delta\theta_2\to f_{r_{P_{12}}}}.$$

Iterate - Outer Loop: $\boldsymbol{\nu}= \mathbf{0}, \mathbf{1}, \mathbf{2}, \ldots; \boldsymbol{\rho} = \boldsymbol{\tau}(\boldsymbol{\nu})$

11) Variable nodes compute marginals according to (36), e.g.:

$$p(\Delta\theta_2) \propto \mathcal{N}(\Delta\hat{\theta}^{\{\nu\}}_2 | \Delta\theta_2, \hat{v}^{\{\nu\}}_{\theta_2})$$

$$\frac{1}{\hat{v}^{\{\nu\}}_{\Delta\theta_2}} = \frac{1}{v_{\theta_2}} + \frac{1}{v^{\{\rho\}}_{f_{r_{P_{12}}}\to\Delta\theta_2}} + \frac{1}{v^{\{\rho\}}_{f_{r_{P_3}}\to\Delta\theta_2}}$$

$$\Delta\hat{\theta}^{\{\nu\}}_2 = \left(\frac{r^{\{\nu\}}_{\theta_2}}{v_{\theta_2}} + \frac{r^{\{\rho\}}_{f_{r_{P_{12}}}\to\Delta\theta_2}}{v^{\{\rho\}}_{f_{r_{P_{12}}}\to\Delta\theta_2}} + \frac{r^{\{\rho\}}_{f_{r_{P_3}}\to\Delta\theta_2}}{v^{\{\rho\}}_{f_{r_{P_3}}\to\Delta\theta_2}}\right)\hat{v}^{\{\nu\}}_{\Delta\theta_2}.$$

12) Variable nodes update the state variables, e.g.:

$$\theta^{\{\nu+1\}}_2 = \theta^{\{\nu\}}_2 + \Delta\hat{\theta}^{\{\nu\}}_2.$$

13) Repeat steps 4-13 until convergence.

Note that, after step 8, initialization factor nodes are removed from the factor graph. Also in each iteration, virtual factor nodes repeat the same message as in the initial step and messages from a virtual factor node to a variable node should not be included in calculation of the marginals.

REFERENCES

[1] A. Abur and A. Expósito, *Power System State Estimation: Theory and Implementation*, ser. Power Engineering. Taylor & Francis, 2004.

[2] F. F. Wu, K. Moslehi, and A. Bose, "Power system control centers: Past, present, and future," *Proceedings of the IEEE*, vol. 93, no. 11, pp. 1890–1908, Nov 2005.

[3] A. Monticelli, *State Estimation in Electric Power Systems: A Generalized Approach*, ser. Kluwer international series in engineering and computer science. Springer US, 1999.

[4] F. C. Schweppe and D. B. Rom, "Power system static-state estimation, part ii: Approximate model," *IEEE Transactions on Power Apparatus and Systems*, vol. PAS-89, no. 1, pp. 125–130, Jan 1970.

[5] Y.-F. Huang, S. Werner, J. Huang, N. Kashyap, and V. Gupta, "State estimation in electric power grids: Meeting new challenges presented by the requirements of the future grid," *IEEE Signal Processing Magazine*, vol. 29, no. 5, pp. 33–43, 2012.

[6] G. N. Korres, "A distributed multiarea state estimation," *IEEE Transactions on Power Systems*, vol. 26, no. 1, pp. 73–84, Feb 2011.

[7] W. Jiang, V. Vittal, and G. T. Heydt, "Diakoptic state estimation using phasor measurement units," *IEEE Transactions on Power Systems*, vol. 23, no. 4, pp. 1580–1589, Nov 2008.

[8] L. Zhao and A. Abur, "Multi area state estimation using synchronized phasor measurements," *IEEE Transactions on Power Systems*, vol. 20, no. 2, pp. 611–617, 2005.

[9] A. Minot, Y. Lu, and N. Li, "A distributed gauss-newton method for power system state estimation," in *2016 IEEE Power and Energy Society General Meeting (PESGM)*, July 2016, pp. 1–1.

[10] D. Marelli, B. Ninness, and M. Fu, "Distributed weighted least-squares estimation for power networks," *IFAC-PapersOnLine*, vol. 48, no. 28, pp. 562–567, 2015.

[11] X. Tai, Z. Lin, M. Fu, and Y. Sun, "A new distributed state estimation technique for power networks," in *2013 American Control Conference*, June 2013, pp. 3338–3343.

[12] R. Ebrahimian and R. Baldick, "State estimation distributed processing [for power systems]," *IEEE Transactions on Power Systems*, vol. 15, no. 4, pp. 1240–1246, 2000.

[13] A. J. Conejo, S. de la Torre, and M. Canas, "An optimization approach to multiarea state estimation," *IEEE Transactions on Power Systems*, vol. 22, no. 1, pp. 213–221, 2007.

[14] S. Boyd, N. Parikh, E. Chu, B. Peleato, and J. Eckstein, "Distributed optimization and statistical learning via the alternating direction method of multipliers," *Foundations and Trends® in Machine Learning*, vol. 3, no. 1, pp. 1–122, 2011.

[15] H. Zhu and G. Giannakis, "Power system nonlinear state estimation using distributed semidefinite programming," *IEEE Journal on Selected Topics in Signal Processing*, vol. 8, no. 6, pp. 1039–1050, 12 2014.

[16] J. Matamoros, A. Tsitsimelis, M. Gregori, and C. Antn-Haro, "Multiarea state estimation with legacy and synchronized measurements," in *2016 IEEE International Conference on Communications (ICC)*, May 2016, pp. 1–6.

[17] V. Kekatos and G. B. Giannakis, "Distributed robust power system state estimation," *IEEE Transactions on Power Systems*, vol. 28, no. 2, pp. 1617–1626, 2013.

[18] X. Li and A. Scaglione, "Robust decentralized state estimation and tracking for power systems via network gossiping," *IEEE Journal on Selected Areas in Communications*, vol. 31, no. 7, pp. 1184–1194, 2013.

[19] L. Xie, D. H. Choi, S. Kar, and H. V. Poor, "Fully distributed state estimation for wide-area monitoring systems," *IEEE Transactions on Smart Grid*, vol. 3, no. 3, pp. 1154–1169, Sept 2012.

[20] A. Gómez-Expósito, A. de la Villa Jaén, C. Gómez-Quiles, P. Rousseaux, and T. Van Cutsem, "A taxonomy of multi-area state estimation methods," *Electric Power Systems Research*, vol. 81, no. 4, pp. 1060–1069, 2011.

[21] J. Pearl, *Probabilistic Reasoning in Intelligent Systems: Networks of Plausible Inference*. San Francisco, CA, USA: Morgan Kaufmann Publishers Inc., 1988.

[22] C. M. Bishop, *Pattern Recognition and Machine Learning*. Springer, 2006.

[23] Y. Weiss and W. T. Freeman, "On the optimality of solutions of the max-product belief-propagation algorithm in arbitrary graphs," *IEEE Transactions on Information Theory*, vol. 47, no. 2, pp. 736–744, Feb 2001.

[24] D. Koller and N. Friedman, *Probabilistic Graphical Models: Principles and Techniques*. MIT Press, 2009.

[25] Y. Hu, A. Kuh, T. Yang, and A. Kavcic, "A belief propagation based power distribution system state estimator," *IEEE Computational Intelligence Magazine*, vol. 6, no. 3, pp. 36–46, 2011.

[26] Y. Weng, R. Negi, and M. Ilic, "Graphical model for state estimation in electric power systems," in *Smart Grid Communications, 2013 IEEE International Conference on*, Oct 2013, pp. 103–108.

[27] T. Sui, D. E. Marelli, and M. Fu, "Convergence analysis of gaussian belief propagation for distributed state estimation," in *Decision and Control (CDC), 2015 IEEE 54th Annual Conference on*. IEEE, 2015, pp. 1106–1111.

[28] F. R. Kschischang, B. J. Frey, and H. A. Loeliger, "Factor graphs and the sum-product algorithm," *IEEE Transactions on Information Theory*, vol. 47, no. 2, pp. 498–519, Feb 2001.

[29] H. A. Loeliger, J. Dauwels, J. Hu, S. Korl, L. Ping, and F. R. Kschischang, "The factor graph approach to model-based signal processing," *Proc. of the IEEE*, vol. 95, no. 6, pp. 1295–1322, 2007.

[30] A. T. Ihler, J. W. Fischer III, and A. S. Willsky, "Loopy belief propagation: Convergence and effects of message errors," *J. Mach. Learn. Res.*, vol. 6, pp. 905–936, Dec. 2005.

[31] A. Monticelli, *State Estimation in Electric Power Systems: A Generalized Approach*, ser. Kluwer international series in engineering and computer science. Springer US, 1999.

[32] D. Barber, *Bayesian Reasoning and Machine Learning*. Cambridge University Press, 2012.

[33] A. Wood and B. Wollenberg, *Power Generation, Operation, and Control*, ser. A Wiley-Interscience publication. Wiley, 1996.

[34] G. Elidan, I. McGraw, and D. Koller, "Residual Belief Propagation: Informed Scheduling for Asynchronous Message Passing," *ArXiv e-prints*, Jun. 2012.

[35] P. Hansen, V. Pereyra, and G. Scherer, "Least squares data fitting with applications." Johns Hopkins University Press, 2012, ch. 9, p. 166.

[36] K. P. Murphy, Y. Weiss, and M. I. Jordan, "Loopy belief propagation for approximate inference: An empirical study," in *Proc. of the 15th Conference on Uncertainty in Artificial Intelligence*, San Francisco, USA, 1999, pp. 467–475.

[37] M. Cosovic and D. Vukobratovic, "State estimation in electric power systems using belief propagation: An extended DC model," in *Signal Processing Advances in Wireless Communications SPAWC, 2016. 17th IEEE Workshop*, Edinburgh, United Kingdom, Jul. 2016.

[38] M. Cosovic and D. Vukobratovic, "Distributed Gauss-Newton Method for AC State Estimation: A Belief Propagation Approach," *ArXiv e-prints*, May 2016.

[39] M. K. Enns, W. F. Tinney, and F. L. Alvarado, "Sparse matrix inverse factors [power systems]," *IEEE Transactions on Power Systems*, vol. 5, no. 2, pp. 466–473, May 1990.

[40] F. L. Alvarado, "Computational complexity in power systems," *IEEE Transactions on Power Apparatus and Systems*, vol. 95, no. 4, pp. 1028–1037, July 1976.

[41] D. Bickson, "Gaussian Belief Propagation: Theory and Aplication," *ArXiv e-prints*, Nov. 2008.